



Published in final edited form as:

J Immunol. 2020 August 15; 205(4): 1084–1101. doi:10.4049/jimmunol.2000181.

ILC2s must partner with the myeloid-macrophage lineage for long-term post-viral lung disease

Kangyun Wu¹, Xinyu Wang¹, Shamus P. Keeler¹, Benjamin J. Gerovac¹, Eugene V. Agapov¹, Derek E. Byers¹, Susan Gilfillan², Marco Colonna², Yong Zhang¹, Michael J. Holtzman^{1,3}

¹Pulmonary and Critical Care Medicine, Department of Medicine, Washington University School of Medicine, St. Louis, MO 63110

²Department of Pathology and Immunology, Washington University School of Medicine, St. Louis, MO 63110

³Department of Cell Biology and Physiology, Washington University School of Medicine, St. Louis, MO 63110

Abstract

Group 2 innate lymphoid cells (ILC2s) are implicated in host defense and inflammatory disease, but these potential functional roles need more precise definition, particularly using advanced technologies to better target ILC2s and engaging experimental models that better manifest both acute infection and chronic even life-long disease. Here we use a mouse model that applies improved genetic definition of ILC2s via *IL7r*-conditional *Rora* gene targeting and takes advantage of a distinct progression from acute illness to chronic disease based on a persistent type 2 immune response to respiratory infection with a natural pathogen (Sendai virus). We first show that ILC2s are activated but are not required to handle acute illness after respiratory viral infection. In contrast, we find that this type of infection also activates ILC2s chronically for IL-13 production and consequent asthma-like disease traits that peak and last long after active viral infection is cleared. However, to manifest this type of disease, *Csf1*-dependent myeloid-macrophage lineage are also active at two levels: first, at a downstream level, this lineage provides lung tissue macrophages (interstitial macrophages and tissue monocytes) that represent a major site of *Il13* gene expression in the diseased lung; and second, at an upstream level, this same lineage is required for *Il33* gene induction that is necessary to activate ILC2s for participation in disease at all, including IL-13 production. Together, these findings provide a revised scheme for understanding and controlling the innate immune response leading to long-term post-viral lung diseases with features of asthma and related progressive conditions.

Address correspondence and reprint requests to Dr. Michael J. Holtzman, Washington University School of Medicine, Campus Box 8052, 660 South Euclid Avenue, St. Louis, MO 63110. Tel. 314-362-8970; Fax: 314-362-9009; mjholtzman@wustl.edu.

Conflict of Interest Disclosures

MJ Holtzman declares that he is a member of the Data Safety Monitoring Board for AstraZeneca and is the founder for NuPeak Therapeutics Inc. The other authors declare no competing financial interests.

1. Introduction

The innate immune system is proving to have new cellular components that orchestrate tissue homeostasis under normal conditions and the response to environmental insults that lead to injury and disease. In particular, there has been a surge in reports on the role of innate lymphoid cells (ILCs) and the special role of group 2 ILCs (designated ILC2s) in the response to infectious and allergenic agents (1). Indeed, some of the first examples of ILC existence and behavior included the immune response to helminth infection and allergen challenge at gut and airway sites in mice (2-8) as a model for what might occur in corresponding human inflammatory diseases such as asthma (9-12). Together, the picture emerged for ILC2s as a key immune component for the development of allergic asthma (13-15). The ILC2 population was also reported to defend against injury due to respiratory viral infections such as influenza A virus (IAV) (16) that is also linked to asthma (17).

However, these initial studies of ILC2s were challenged by the difficulty in specific definition of ILC2 function, generally based on genetic deletion. This challenge has continued into the latest round of studies using *Rag2^{-/-}Il2rg^{-/-}*, *Bcl11b^{flox/-}*, or *Plzf^{-/-}* mice (13, 18-25) and *Il7ra-Cre* mice without an additional cell-specific floxed-target gene (26, 27). A recent advancement has been the combination of *Il7ra-Cre* crossed to *Rora-flox* transgenic mice to more selectively eliminate ILC2s (28, 29), taking advantage of requirements specific for ILC2s (30-32) and avoiding complications of *Rora*-deficiency at other cell sites (33). Thus, the application of *Il7ra-Cre-Rora-flox* mice was used successfully to define a role for ILC2s to partner with CD4⁺ Th2 cells in the type 2 immune response against helminth infection and with Th2 and dendritic cells in the immune memory response to allergen (28, 29). However, this technical advance has not been applied to the key issues of host defense and chronic inflammatory disease. Indeed, the role of ILC2s remains undefined in long-term models in general, leaving uncertainty for the pathological role for ILC2s alone and in combination with other immune and stromal cell populations (1).

To address these issues, the current study engaged mice that were bred as *Il7ra^{wu/Cre}-Rora^{fl/fl}* mice to achieve more selective and efficient deletion of ILC2s. In addition, we employed a mouse model that manifests both acute illness and subsequent progression to chronic inflammatory disease after infection with the natural mouse pathogen Sendai virus (SeV) (34-37). To date, the SeV model appears similar to the response to human pathogens such as influenza A virus (IAV) and respiratory enterovirus (EV-D68) in mice (17, 37) and the type 2 immune response found in humans with lung disease due to asthma and chronic obstructive pulmonary disease (COPD) (34, 35, 38, 39). Together, the present approach offered opportunities not found in models that lack long-term disease and ILC2-specific targeting (40-42) and thereby provided for a series of unexpected findings to establish a distinct paradigm for ILC2 engagement in host defense and inflammatory disease in collaboration with neighboring niches of myeloid and epithelial cell populations.

Materials and methods

Mice

Male and female wild-type C57BL/6J mice (000664) mice were obtained from The Jackson Laboratory. The *Il7ra^{wt/Cre}-Rora^{fl/fl}* mice were bred by crossing *Il7ra^{wt/Cre}* and *Rora^{fl/fl}* generated as described previously (28, 29) with the *Rora^{fl/fl}* mice kindly provided by Andrew McKenzie (Cambridge, UK) and the *Il7ra*-Cre mice by Hans-Reimer Rodewald (German Cancer Research Center, Heidelberg, GDR). The *Il13^{wt/gfp}* mice were initially generated as described previously (7) and were also kindly provided by Andrew McKenzie. The *op/opT* mice were generated as described previously (43) and were kindly provided by Nandini Ghosh-Choudhury (University of Texas, San Antonio). These mice were crossed to wild-type mice to generate heterozygous *wt/opT* mice and littermate *wt/wt* control mice as described previously (36). The *Il33^{cherry/cherry}* mice were generated with insertion of an mCherry-reporter cassette between exons 4 and 5 of the *Il33* gene in ES cells from C57BL/6J mice. Levels of IL-33 expression were checked with goat anti-mouse IL-33 Ab (R&D Systems, AF3626) for western blotting of lung tissue samples as described previously (44). All mouse strains were maintained on a C57BL/6J genetic background and except where indicated were studied as the gene-targeted strain compared to littermate control mice housed under the same conditions.

Mouse model

All mice were maintained and co-housed in a barrier facility using cages fitted with micro-isolator lids. Animal husbandry and experimental procedures were approved by the Animal Studies Committees of Washington University School of Medicine in accordance with the guidelines from the National Institutes of Health. SeV was obtained from ATCC (Sendai/52 Fushimi strain, ATCC VR-105) and prepared and titered by plaque-forming assay and qPCR assay as described previously (34). Mice were infected with SeV (2.6×10^5 PFU) as described previously (37). Dosing was performed intranasally using SeV in 30 μ l of PBS or an equivalent amount of UV-inactivated virus or PBS alone under ketamine/xylazine anesthesia at 6-9 wk of age. Results from male and female mice were pooled since no significant differences were found between sexes as reported initially (45) and confirmed recently (37) and in the present experiments (data not shown). Viral titers for stock solutions and lung infections were monitored by PCR assay using primers defined previously (37). All animals undergo daily cage side observation for clinical behavior and food consumption.

Flow cytometry

Single cell suspensions were generated from minced lung tissue that was subjected to collagenase (Liberase TM Research Grade, Roche), hyaluronidase (Sigma), DNase I (Sigma), and Dispase II (Roche) digestion for 45 min at 37 °C and then treated with ACK buffer (Lonza) to remove red blood cells. Following FcR blockade, lung cell suspensions were incubated with labeled antibodies and were sorted using a Sony SY3200 Synergy high-speed cell sorter. The following antibodies were used: anti-mouse CD31 (clone MEC 13.3; BD Biosciences), anti-mouse CD45 (clone 30-F11; BD Biosciences), anti-mouse EpCAM (clone G8.8; BioLegend), anti-mouse F4/80 (Clone BM8; eBiosciences), anti-mouse Ly6G (Clone 1A8, BD Biosciences), anti-mouse CD11c (Clone HL3; BD Biosciences), anti-

mouse Siglec F (Clone E50-2440; BD Biosciences), anti-mouse CD11b (Clone M1/70; BD Biosciences), Mouse Lineage Antibody cocktail (BD Biosciences), anti-mouse 90.2 (Clone 53-2.1; BD Biosciences), anti-mouse ST2 (Clone DIH9; BioLegend), anti-mouse CD25 (Clone PC61; BD Biosciences), anti-mouse CD117 (Clone 2B8, BD Biosciences), anti-mouse CD278 (Clone 7E.17G9, BD Biosciences), anti-mouse 6A/E (Clone E13-161.7, BD Biosciences), anti-mouse MHCII (Clone M5/114.15.2, eBiosciences), anti-mouse CD3e (Clone 145-2C11, BD Biosciences), anti-mouse NK1.1 (Clone PK136, BD Biosciences), and anti-GFP (Clone 1A12-6-18, BD Biosciences). Flow cytometry results were plotted and analyzed using FlowJo software (TreeStar).

Immunostaining

Cells were fixed and permeabilized, and lung sections were incubated with citrate-based antigen unmasking solution for antigen retrieval as described previously (38). Immunostaining was performed using the following antibodies: chicken anti-GFP (Abcam), rat anti-mouse F4/80 (clone CI:A3-1; Abcam), rabbit anti-human GATA-3 (clone D13C9, Cell Signaling Technology, goat anti-mouse IL-13 (R&D systems), and goat anti-mouse IL-33 (R&D systems). Antibody binding was visualized using Alexa 488 or 594 conjugated secondary antibody (Life Technologies). All slides were also counterstained with Prolong Gold with DAPI (Life Technologies) and then imaged by immunofluorescent microscopy using a Leica DM5000 B microscope. Staining was quantified in whole lung sections using a NanoZoomer S60 slide scanner (Hamamatsu) and ImageJ software.

Real-time quantitative PCR assay

RNA was purified from lung homogenates and cells using Trizol (Invitrogen) and was converted to cDNA using a High-Capacity cDNA Archive kit (Life Technologies). Target mRNA was quantified by real-time PCR assay using specific fluorogenic probes and primer sets and the Fast Universal PCR Master Mix system (Applied Biosystems). The forward and reverse primers and probes for *SeV-NP* were 5'-GGCGGTGGTGAATTGAG-3', 5'-CATGAGCTTCTGTTTCTAGGTCGAT-3', 5'-AGCTCTAGACAATGCC-3'; for *Il13* were 5'-GGTGCCAAGATCTGTGTCTC-3', 5'-CCACACTCCATACCATGCTG-3', 5'-AAGACCAGACTCCCCTGTGCAAC-3'; for *Muc5ac* were 5'-TACCACTCCCTGCTTCTGCAGCGTGCA-3', 5'-ATAGTAACAGTGGCCATCAAGGTCTGTCT-3', 5'-TATACCCCTTGGGATCCATCATCTACA-3'; for *Arg1* were 5'-AGTGTGATGTCAGTGTGAGC-3', 5'-GAATGGAAGAGTCAGTGTGGT-3', 5'-ACAGTCTGGCAGTTGGAAGCATCT-3'; for *Il33* were 5'-TCATGTTACCATCAGCTTCT-3', 5'-GTGCTACTACGCTACTATGAGTC-3', 5'-ACCGTCGCCTGATTGACTTGCA-3'; for *Il12b* were 5'-TGTCCTCAGAAGCTAACCATC-3', 5'-TCCAGTCCACCTCTACAACA-3', 5'-ACGCTTTTCTCCAGCTCCCACATG-3'; for *Gata3* were 5'-CCTTATCAAGCCCAAGCGAA-3', 5'-GTCCCCATTAGCGTTCCCTC-3', 5'-TGTCCCTGCTCTCCTTGCTGC-3'; for *Rora* were 5'-TGGAGACAAATCGTCAGGAATC-3', 5'-GACAGGAGTAGGTGGCATTG-3', 5'-TGG TGT CATTAC GTG TGA AGG CTG C-3'; for *Il1rl1* were 5'-AAT CCT CCA TAC AAC CAC ACA A-3', 5'-GACATCAGCCAAGAAGTGAGAG-3', 5'-AAGTAT

TGCCTGTTTCAGCTTGCTTTGG-3'; for *Areg* were 5'-GTCACATATCTTTGTCTCTGCCA-3', 5'- CCTCCTTCTTTCTTCTGTTTCTCC-3', 5'- AGTATCGTTTCCAAAGGTGCACTGTGA-3'. Samples were assayed with the 7300HT or QuantStudio 6 Fast Real-Time PCR System and analyzed using Fast System Software (Applied Biosystems). All real-time PCR data was normalized to the level of *GAPDH* mRNA. Values were expressed as fold-change based on the delta-delta Ct method as described previously (35) with the exception of Fig. 3f where *Il13* mRNA was quantified by copy number using an *Il13*-expressing plasmid as an internal standard (38).

ELISA

For IL-33 production in lung tissues, mouse lungs were homogenized in RIPA buffer (Sigma) supplemented with protease inhibitor cocktail (Roche) and 1 mM EDTA. For IL-33 production in bronchoalveolar lavage (BAL), mouse lungs were washed twice with 1 ml of PBS on ice. The samples from each mouse were pooled, spun to remove cells, supplemented with protease inhibitor cocktail and 1 mM EDTA. Levels of IL-33 were determined using the Duoset ELISA kit (R&D Systems).

Statistical analysis

All data are presented as mean and s.e.m. and are representative of at least three experiments with at least 5 data points per experiment. Unpaired student's t-test with Bonferroni correction as well as mixed-model repeated measures analysis of variance with Tukey correction for multiple comparisons were used to assess statistical significance between means. In all cases, significance threshold was set at $P < 0.05$.

Results

ILC2s do not influence acute respiratory viral infection

Initial experiments established the presence of ILC2s in the lung at baseline using flow cytometry for forward scatter (FS) and side scatter (SS) combined with absence of immune cell lineage markers (CD11c, NK1.1, CD3e, CD45R/B220, CD11b, TER-119, and Ly6G/6C) and presence of CD90.2 (alloantigen Thy-1.2) and ST2 (IL-33R subunit IL-1r11) (Fig. 1a). This cell population also expressed CD25 (IL-2 α), CD117 (c-Kit), CD127 (IL-7 α), CD278 (ICOS), Lys6A/E (Sca1), and MHC-II based on additional flow cytometry analysis (Fig. 1b). Together, this profile for ILC2s is similar to reports using the comparable methods (16, 29, 46, 47). Moreover, this ILC2 population was no longer detected in the lungs of *Il7ra^{wt/Cre}-Rora^{fl/fl}* mice that were designed to specifically delete ILC2s (Fig. 1c). ILC2 deficiency was consistent with previous work using this genetic approach (28, 29).

These findings allowed us to next test the effect of ILC2 deficiency on the outcome from respiratory viral infection. As introduced above, we used SeV, as a natural mouse pathogen capable of replicating at high efficiency and causing acute infectious illness across outbred and inbred strains (including C57BL/6J). In this setting, we found no significant changes in the typical weight loss, viral RNA level and clearance, or immune cell accumulation in *Il7ra^{wt/Cre}-Rora^{fl/fl}* mice compared to wild-type (WT) control mice (Fig. 1d-f). Similarly, we found no significant differences in ILC2-deficient mice in *Il12b* mRNA (Fig. 1g) as a

validated marker of acute inflammation after SeV infection (48). In addition, we detected no significant differences in amphiregulin (*Areg*) mRNA level in ILC2-deficient mice except for a slight decrease at 12 d after infection (Fig. 1g). However, by this time, repair of epithelial injury and clearance of infectious virus are already complete (37, 49). Thus, the results are consistent with normal recovery in ILC2-deficient mice as noted above (Fig. 1d-f). In addition, we detected attenuation of the usual increase in lung levels of *Il13* mRNA at the time of peak viral titer (5 d after infection) and not at other time points (Fig. 1g), consistent with a transient type 2 immune response found after viral infection and the role of ILC2s in IL-13 production during acute activation in gut and lung (4, 5, 7, 8, 10).

ILC2s contribute to chronic lung disease after viral infection

We next studied the behavior and influence of ILC2s during the development of chronic lung disease that develops after clearance of active viral infection. For SeV infection, chronic disease becomes detectable at 21 d and maximal at 49 d after infection as key time points for study (34, 35, 37, 50). This strategy showed that the levels of ILC2s in the lung were increased markedly at 21 and 49 d after SeV infection in WT mice and were more pronounced than the increases at 5 d after infection or the overall increases in total cell numbers that are typical of acute illness and chronic lung disease (Fig. 2a). In addition, ILC2s that were FACS-purified from the lung showed an increased induction of ILC2 biomarkers *Il13*, *Gata3*, and *Rora* mRNA in response to IL-33 stimulation at 49 d after SeV infection compared to SeV-UV controls (Fig. 2b). As expected, the increase in ILC2s found in WT mice was markedly attenuated in *Il7ra^{w^t/Cre}-Rora^{fl/fl}* mice based on flow cytograms at 49 d after infection (Fig. 2c). Together, these findings provided for ILC2 accumulation and activation in concert with the development and progression of chronic lung disease after viral infection.

To pursue any possible function of ILC2s in the development of chronic lung disease, we next compared WT to *Il7ra^{w^t/Cre}-Rora^{fl/fl}* mice for signs of this disease at 49 d after SeV infection. Consistent with ILC2 accumulation and activation with disease, we found significant attenuation of hematoxylin⁺ cell-staining (a sign of focal immune and epithelial cell accumulation) in lung sections from *Il7ra^{w^t/Cre}-Rora^{fl/fl}* compared to WT mice at 49 d after SeV infection (Fig. 2d,e). Similarly, we found attenuation of increased PAS⁺ staining (a sign of focal mucus production) in lung sections from *Il7ra^{w^t/Cre}-Rora^{fl/fl}* compared to WT mice (Fig. 2f,g). In concert with these observations, we also detected reduction of the usual increases in *Il13*, *Muc5ac*, and *Arg1* mRNA levels (as signs of a type 2 immune response and mucus production) in the lungs of *Il7ra^{w^t/Cre}-Rora^{fl/fl}* compared to WT mice at 49 d after SeV infection (Fig. 2h). Together, the findings established a significant role for ILC2s in the development of chronic lung disease after viral infection. However, we also recognized that the degree of attenuation in *Il7ra^{w^t/Cre}-Rora^{fl/fl}* mice was incomplete in comparison to *Il13^{-/-}* mice for all phenotypes, i.e., hematoxylin⁺ staining (Fig. 2d,e), PAS⁺ staining (Fig. 2f,g), and *Il13*, *Muc5ac*, and *Arg1* mRNA levels (Fig. 2h). These results indicated that ILC2 deficiency alone cannot fully block the development of chronic lung disease after viral infection, and the remaining effect might be due at least in part to a separate cellular mechanism for IL-13 production in this setting.

ILC2s and macrophages contribute to IL-13 production

Our previous work indicated that lung macrophages (but not mast cells, basophils, neutrophils, dendritic cells, B cells, CD4⁺ T cells, CD8⁺ T cells, NK cells, or NKT cells) can also be a source of increased IL-13 production after viral infection based on PCR-assay for *Il13* mRNA and immunostaining for IL-13, and thereby contribute to the development of chronic lung disease after SeV infection (34, 36). To more precisely define the cellular source of IL-13, here we studied IL-13-GFP reporter mice, using heterozygous *Il13^{wt/gfp}* mice that manifest the same degree of acute illness and chronic lung disease as wild-type control (*Il13^{wt/wt}*) mice after SeV infection (data not shown). Accordingly, we found a similarly increased percentage of lineage⁻ST2⁺CD90.2⁺ ILC2s in lungs of *Il13^{wt/wt}* and *Il13^{wt/gfp}* mice at 49 d after SeV infection compared to SeV-UV control based on flow cytograms from these conditions (Fig. 3a). In addition, we found a marked increase in GFP⁺ ILC2s at 49 d after SeV infection compared to SeV-UV in lungs of *Il13^{wt/gfp}* mice, and both of these values were increased compared to background levels found in WT mice (Fig. 3a). Similarly, we found high-level IL-13 expression marked by GFP fluorescence in ILC2s from the lungs of *Il13^{wt/gfp}* mice compared to *Il13^{wt/wt}* mice, and this signal was significantly increased at 49 d after SeV compared to SeV-UV control based on mean fluorescence intensity (MFI) (Fig. 3b,c).

We also checked for GFP expression in lung macrophage populations based on flow cytometry schemes that separated these populations into alveolar macrophages (Ly6G⁻CD11c⁺Siglec-F⁺F4/80⁺CD11b⁻) and tissue macrophages (Ly6G⁻CD11c⁻Siglec-F⁻F4/80⁺CD11b⁺) and further separated tissue macrophages into interstitial macrophages and tissue monocytes based on differences in cell size (Fig. 4a,b). In contrast to results with ILC2s, we found no detectable GFP⁺ population of macrophages (alveolar or tissue subsets) at 49 d after SeV infection compared to SeV-UV control using detection of fluorescence directly from GFP or anti-GFP mAb (Fig. 4c,d). As expected from our previous work (34), we also found no detectable IL-13-GFP signal in NKT cells (SS^{low}CD3e⁺NK1.1⁺) or T cells (SS^{low}CD3e⁺) (Fig. 4c,d). Similarly, we found no significant IL-13-GFP signal in eosinophils (Ly6G⁻CD11c⁻Siglec-F⁺F4/80⁻CD11b⁺) (Fig. 4c,d) that contribute to IL-13 production in other models (51). Together, these findings again show that IL-13-expressing ILC2s were recruited and activated during the chronic lung disease that develops after SeV infection but did not as yet identify alternative cell sources of IL-13 production.

To investigate this issue, we developed additional approaches that might better define any role for lung macrophages as a source of IL-13 production in this model (34, 36), especially relative to ILC2s and in relation to macrophage subsets. Accordingly, we combined FACS of alveolar and tissue macrophages with PCR-based assay for *Il13* mRNA to establish cell-type sites of IL-13 expression. Similar to the results from the IL-13-GFP-reporter approach, we found that the level of *Il13* mRNA per cell at baseline (without SeV infection) and after induction at 5 d and 49 d after SeV infection was highest in lung ILC2s compared to macrophages, where only low levels could be detected in tissue macrophages at 49 d after infection (Fig. 5a). To further define the site of IL-13 production, we also determined IL-13 protein levels in bronchoalveolar lavage fluid (BALF) and lung tissue. This approach demonstrated increases in IL-13 levels in both compartments at 5 d and 49 d after SeV

compared to SeV-UV in WT mice, and these increases were attenuated in ILC2-deficient *I17ra^{wt/Cre}-Rora^{fl/fl}* mice (Fig. 5b). However, despite the selective increase in *Il13* mRNA in ILC2s, the loss of ILC2s did not fully block IL-13 production in the lung or release into the airway/alveolar space after SeV infection. This finding again raised the possibility for another cellular source of IL-13 in the lung, with the tissue macrophage as a particular candidate.

To address this issue, we compared *Il13* mRNA levels in the chief cell sources (tissue macrophages and ILC2s) as mRNA copy number per cell and per lung. Using this comparison in our analysis of *Il13* mRNA per cell, we again found a relatively low level of *Il13* mRNA in tissue macrophages compared to ILC2s (Fig. 5c). However, when we expressed *Il13* mRNA as levels per lung (where lung level = level per cell x number of cells per lung), we recognized that more abundant tissue macrophages are the main site of *Il13* mRNA expression at 49 d after SeV infection (Fig. 5c). In fact, the fold-increase and overall level of *Il13* mRNA in the lung at 49 d after SeV infection was significantly higher for tissue macrophages than ILC2s (Fig. 5c). The comparative analysis for eosinophils (gated as shown in Fig. 4a) showed *Il13* mRNA levels similar to tissue macrophages, but eosinophil number was not sufficient to provide a substantial contribution to *Il13* expression in the lung (Fig. 5c). As introduced above, the larger number of lung macrophages was also accompanied by increased post-viral induction of *Il13* gene expression with 21-fold in tissue macrophages compared to 5.2-fold in ILC2s and 5.1-fold in eosinophils.

To further assign production of IL-13 to macrophages, we also performed immunostaining for IL-13 protein production in lung tissue and FACS-isolated cells. Tissue immunostaining for IL-13 itself might not discriminate sites of cell production versus cell binding or uptake. We overcame this difficulty by staining for GFP expression in *Il13^{w^t/gfp}* mice. This approach showed cells with tissue macrophage morphology and location and dim staining as well as cells with ILC2 morphology and bright staining for IL-13-GFP with no background signal with GFP only staining (Fig. 5d). Cells identified as ILC2s by GFP-staining intensity and morphology were also found to immunostain positive for GATA3 (Fig. 5e), as a marker of type 2 lymphocytes. Further, this approach showed that cells with macrophage morphology and location were not stained for GATA3 (Fig. 5e) but instead were co-stained for IL-13-GFP and F4/80 in lung sections from *Il13^{w^t/gfp}* mice at 49 d after SeV infection but only for F4/80 in SeV-UV control mice (Fig. 5f). These results were similar to macrophage immunostaining for IL-13 in previous work (34-36). Here again, we identified cells with lymphoid morphology that were stained even more brightly for IL-13-GFP but were not co-stained for F4/80 (Fig. 5f), consistent with identification as IL-13-expressing ILC2s. Image-analysis quantitation of tissue immunostaining indicated that GFP⁺F4/80⁺ cells (consistent with IL-13-expressing tissue macrophages) were far more abundant than GFP⁺F4/80⁻ cells (consistent with IL-13-expressing ILC2s) (Fig. 5g). As introduced above, we also checked for IL-13 expression in FACS-isolated tissue macrophages, in this case by immunostaining with anti-mouse IL-13 Ab that can define IL-13 production in preparations of purified cells. Here again, we demonstrated that tissue macrophages defined by flow cytometry and morphology characteristics were immunostained for IL-13 when obtained from the lungs at 49 d after SeV but not after SeV-UV control (Fig. 5h). Together, these results provided evidence for marked induction of *Il13* gene expression in tissue macrophages during chronic

lung disease after viral infection and for this population along with ILC2s to represent prominent sites of IL-13 production. This combined contribution might therefore lead to an increased concentration-dependent effect of IL-13 to better explain continued IL-13-dependent lung disease despite ILC2-deficiency (Fig. 2d-h).

ILC2 activation depends on myeloid-macrophage input to ST2

To further address macrophage contribution to IL-13 production, we next incorporated a genetic strategy for targeted *Csf1*-deficiency that would markedly down-regulate the myeloid-macrophage lineage and in turn tissue macrophage levels. For this approach, we started with *Csf1^{op/opT}* (*op/opT*) mice that carry an osteocalcin-driven *Csf1* transgene (*T*) that rescues the osteopetrosis but not the macrophage defect in *Csf1^{op/op}* (*op/op*) mice (43). We then generated heterozygous *Csf1^{wt/opT}* (*wt/opT*) mice that still manifest a significant decrease in the level of lung tissue macrophages (i.e., interstitial macrophages plus tissue monocytes) and attenuation of chronic lung disease (36). Comparison of *wt/opT* to littermate wild-type (*wt/wt*) mice can therefore provide an indication of tissue macrophage contribution to phenotype, including IL-13 expression. In this setting, we found no significant changes in the typical weight loss, viral RNA level and clearance, or immune cell accumulation in *wt/opT* mice compared to *wt/wt* mice (Fig. 6a-c). These results indicated that down-regulation of the myeloid-macrophage lineage did not significantly influence acute illness after viral infection, similar to the case for ILC2 deficiency.

In contrast to the results for acute illness, we detected informative differences in the development of chronic disease in *wt/opT* mice. In particular, we found that the increased levels of *Il13* mRNA were localized selectively to both subsets of tissue macrophages and that *Il13* mRNA induction was markedly down-regulated in *wt/opT* compared to *wt/wt* mice (Fig. 6d). The IL-13-target *Arg1* mRNA was up-regulated in both alveolar and tissue macrophages in corresponding WT mice (i.e., *wt/wt* mice), and this effect was fully blocked in *wt/opT* mice (Fig. 6d). These results were consistent with our earlier observations that tissue macrophages were sensitive to *Csf1*-dependent down-regulation (36), in this case leading to decreases in *Il13* and *Il13*-dependent gene expression.

To further define macrophage control of IL-13 production, we also determined the levels of ILC2 recruitment and activation in the lungs of *wt/opT* mice compared to *wt/wt* mice. Unexpectedly, we found first that the increased percentage of Lin⁻CD90.2⁺ST2⁺ ILC2s at 49 d after SeV in *wt/wt* mice was attenuated in *wt/opT* mice without a significant change in baseline percentages after SeV-UV (Fig. 6e). Quantitation of flow cytometry analysis showed the usual increase in total cell number after SeV infection in *wt/opT* mice (Fig. 6f) that was similar to *wt/wt* mice (Fig. 2a). We also detected an increase in ILC2 levels at 5 d after SeV infection in *wt/opT* (Fig. 6f), again similar to *wt/wt* control mice (Fig. 2a). However, the marked increases in ILC2 levels in the lung at 21 and 49 d after SeV infection found in *wt/wt* mice (Fig. 2a) were no longer significant in *wt/opT* mice (Fig. 6f), recognizing that ST2 expression can represent cell number and activation as contributions to cell function. We did not find a significant difference in ILC2 levels in *wt/opT* compared to *wt/wt* mice (Fig. 6f versus Fig. 2a) at any timepoint in SeV-UV controls, indicating that

there was no defect in ILC2 development and migration to the lung tissue under baseline conditions.

Similar to the results for ILC2 levels, we found that the usual induction of *Il13* and *Arg1* mRNA found in ILC2s from the lungs of *wt/wt* mice were fully blocked in *wt/opT* mice at 49 d after SeV (Fig. 6g). Further, the levels of *Gata3* and *Il1rl1* mRNA (the latter encoding for the IL-33 receptor designated ST2) were markedly down-regulated in ILC2s from *wt/opT* mice at 49 d after SeV or SeV-UV (Fig. 6g). In contrast to *Il1rl1* mRNA, levels of ST2 protein on ILC2s were up-regulated at 49 d after SeV infection, and this effect was fully blocked in *wt/opT* mice based on cell counts (Fig. 6h) or MFI (Fig. 6i). Similar induction of ST2 expression after SeV infection was also found on tissue macrophages based on flow cytometry analysis by histogram and cytogram (Fig. 7a,b), albeit on a smaller subset of this cell population compared to broad expression across the ILC2 population (Fig 6h). Nonetheless, both findings suggested a basis for enhanced ST2-dependent activation of ILC2s and tissue macrophages for IL-13 production and for the unexpected role of *Csfl*-dependent myeloid cells in controlling ILC2 accumulation and activation as a distinct mechanism for chronic lung disease after viral infection. Moreover, the loss of myeloid cell input resulted in a targeted decrease in *Il1rl1*/ST2 expression and consequent down-regulation of the type 2 immune response as marked by *Il1rl1*, *Gata3*, and ST2 levels after viral infection in *wt/opT* mice.

ILC2 activation via ST2 depends on IL-33 production

To further develop this new disease mechanism, we next sought to define the basis for increased ST2 expression and the impact on ST2 signaling function after viral infection. As introduced above, we recognized that ST2 signal transduction was required for induction of *Il13* gene expression, and this signal depended on IL-33 as ST2-receptor ligand in the present and previous mouse models wherein mucus production is markedly attenuated by anti-ST2 mAb or *Il1rl1* or *Il33* gene targeting (35, 52). To better define this issue, we generated IL-33-deficient mice wherein a cherry-reporter gene cassette was inserted between exons 4 and 5 of the *Il33* gene (Fig. 8a,b). Accordingly, homozygous *Il33^{cherry/cherry}* mice were unable to generate any detectable IL-33 protein in the lung at 49 d after SeV infection or SeV-UV (Fig. 8c). Nonetheless, the acute illness after SeV infection was no different in *Il33^{cherry/cherry}* mice compared to *Il33^{wl/wl}* mice based on cage side observation, body weight loss, viral RNA level, and histopathology (Fig. 8d-f). These results are also similar to our previous findings using *Il33^{Gt/Gt}* mice that show no differences from WT mice in these same parameters after SeV infection (35).

Despite similarities in acute illness, the development of chronic lung disease marked by the usual increases in inflammatory cells and PAS⁺ airway mucous cells in lung sections (Fig. 9a,b) and in levels of *Il13* and *Arg1* mRNA in lung tissue (Fig. 9c) were all significantly attenuated in *Il33^{cherry/cherry}* mice compared to *Il33^{wl/wl}* mice at 49 d after SeV infection. In addition, lung levels of *Gata3* and *Il1rl1* mRNA were decreased in *Il33^{cherry/cherry}* mice after SeV and SeV-UV (Fig. 9c). The same pattern of down-regulated gene expression was found in ILC2s from *Il33^{cherry/cherry}* mice (Fig. 9d), in concert with decreased levels found in ILC2s from *wt/opT* mice (Fig. 6g). In addition, we found that the increased percentage of

ILC2s in the lungs of *Il33^{wt/wt}* mice at 49 d after SeV infection was also significantly down-regulated in *Il33^{cherry/cherry}* mice based on flow cytometry analysis for Lin⁻CD90.2⁺ ST2⁺ ILC2s (Fig. 9e). Quantitation of this analysis confirmed that the marked increases in the numbers of ILC2s in the lungs at 21 and 49 d after SeV infection in *Il33^{wt/wt}* mice were significantly decreased in *Il33^{cherry/cherry}* mice (Fig. 9f). This analysis also demonstrated a slight decrease in ILC2 levels in *Il33^{cherry/cherry}* compared to *Il33^{wt/wt}* mice at baseline in SeV-UV controls (Fig. 9f), consistent with the relatively small effect of IL-33 on ILC2 development in the bone marrow and migration to the lung tissue under baseline conditions (53). In follow-up to the attenuation of ILC2 levels, we also observed that the increased levels of ST2 on ILC2s at 49 d after SeV infection in *Il33^{wt/wt}* mice were no longer found in *Il33^{cherry/cherry}* mice based on cell counts (Fig. 9g) and MFI (Fig. 9h). Together, these findings indicated that IL-33 production was a suitable candidate for *Csf1*-dependent myeloid cell control of ILC2 accumulation and activation for chronic lung disease after viral infection.

IL-33 production depends on myeloid-macrophage lineage input

We next aimed to determine whether in fact myeloid cells could control IL-33 production as a mechanism to regulate the development of disease after viral infection. As a first step, we combined a flow cytometry scheme for separating CD31⁻CD45⁻EpCam⁺ lung epithelial cells (Fig. 10a) with our scheme for lung macrophages (Fig. 4a) to track quantitatively the cell site of IL-33 expression. This combined analysis showed that *Il33* mRNA was almost entirely confined to lung epithelial cells at baseline levels without infection and at increased levels at 49 d after SeV infection (Fig. 10b). This finding was consistent with the predominant site of IL-33 expression in the mouse lung being localized to alveolar epithelial type 2 (AT2) cells based on cell and tissue morphology and co-expression with AT2 cell markers such as surfactant protein C (*Sftpc*) (35, 52, 54, 55). Indeed, we also found increases in IL-33⁺ immunostaining localized to cells with AT2 cell morphology and location in *wt/wt* mice at baseline (Fig. 10c). No such immunostaining was found in *Il33*-deficient *cherry/cherry* reporter mice as a sign of specificity for IL-33 detection. This approach also showed that IL-33⁺ immunostaining was increased in *wt/wt* mice at 49 d after SeV compared to SeV-UV, and this increase was attenuated in *wt/opT* mice (Fig. 10c). These findings were confirmed as significant with quantitation of IL-33⁺ cell levels in lung tissue (Fig. 10d). In addition, we found that the usual increase in *Il33* mRNA and consequent increase in *Il13* mRNA at 49 d after SeV infection in the lungs of *wt/wt* mice were no longer detectable in *wt/opT* mice (Fig. 10e). Together, these results are consistent with an effect of *Csf1*-dependent myeloid cells to promote epithelial cell expression of IL-33 (in lung epithelial cells) that in turn drives downstream IL-13 production and feed-forward ST2 expression (in ILC2s and tissue macrophages) that are all critical for the development of chronic lung disease after viral infection.

Discussion

Here we apply improved genetic technologies and a distinct mouse model to define the role of ILC2s in acute illness and chronic disease after respiratory viral infection. Relative to previous work, the present study provides a series of unexpected conceptual advances. In

particular, we show that ILC2s are activated during respiratory viral infection with a natural mouse pathogen (SeV) but are not required to handle acute illness and recovery from this type of infection. In contrast, we find that this type of infection also activates ILC2s chronically for IL-13 production that is required for the development of long-term post-viral lung disease with features of asthma and COPD. Notably, however, ILC2s require critical activities of *Csf1*-dependent myeloid cells at two levels: first, at a downstream level for significant additional IL-13 production; and second, at an upstream level for enhanced IL-33 expression that is essential for ILC2 participation at all in the development of disease. Together, these findings provide a revised scheme (as depicted in Fig. 11) that appears distinct from the conventional view of an innate immune response engineered for short-term versus long-term activation and function. This alternative paradigm thereby provides a new framework for understanding and controlling the innate immune response to viral infection and likely other stimuli of the type 2 immune response. Here we discuss several of our observations that are critical to this issue.

First, we address the possible function of ILC2s in host defense against respiratory viral infection. As noted in the *Introduction*, ILC2s were reported to be responsible for clinical deterioration via poor epithelial repair after infection with IAV (PR8 strain) based on ILC2 depletion using anti-CD90.2 mAb in *Rag*^{-/-} mice (16). More recently, another group found decreased survival after IAV (California/04/2009 strain) infection based on ILC2 depletion with *Il7ra-Cre-Rora-flox* mice (56). The combined studies of IAV implicate an IFN γ -IL-5-amphiregulin axis for the ILC2-dependent phenotype after IAV infection. Similarly, others find a role for IL-33-IL-33R signal transduction (that should activate ILC2s) in defense against IAV infection (16, 56). In contrast, we found no detectable effect of ILC2 depletion on recovery from acute illness (or induction of amphiregulin expression during tissue repair) and no effect of IL33 or IL-33R deficiency on acute illness in the present or previous work on SeV infection (35). Whether the low number and/or activation of ILC2s and consequent absence of function during acute illness found in our model is present in other conditions is uncertain. Nonetheless, there are no reported increases in susceptibility to severity of respiratory viral infections in humans treated with mAbs that block IL-5-IL-5R or IL-33-IL-33R signal transduction (57-59), and IFN- γ -deficient humans are limited to susceptibility to mycobacterial infection (60). Our results are also consistent with normal susceptibility to viral infection in ILC-deficient humans (61). Thus, it is possible that ILC2s might manifest a distinct role specific to IAV infection adapted to mice, recognizing that studies of this issue are ongoing.

Second, we address the key question of ILC2 function in chronic inflammatory disease. Here we took special advantage of the capacity of SeV infection to trigger long-term lung disease lasting the 1-2 year lifespan of mice (50), analogous to epidemiology data that links severe respiratory viral infection in infancy to lifelong lung disease in humans (62). Consistent with these observations, we find that ILC2s are activated persistently after viral infection, thereby providing a basis for contributing to chronic lung disease that develops long after infectious virus is cleared. This prolonged time course is distinct from reports of short-term ILC2 activation after other stimuli, e.g., allergen-challenge and infections with helminths and respiratory viruses in mice (4, 5, 7, 8, 10, 41, 42) and recently in humans (63). These studies often focused on the ILC2 population as a source of IL-13 production and

therefore a driver for IL-13-dependent disease that is characteristic of a type 2 immune response. Here we also find that the ILC2s exhibit high-level IL-13 expression in concert with the later development and progression of lung disease after viral infection. However, we also discover two distinct features of the ILC2-based disease paradigm.

One of those elements is the observation that ILC2s cannot fully account for IL-13 production that develops during post-viral lung disease. This observation led us to identify tissue monocytes and interstitial macrophages (that together we designate as tissue macrophages) as an additional site for induction of *Il13* gene expression during chronic lung disease after viral infection. The present approach incorporated ILC2-deficient mice to quantify the contribution to lung IL-13 levels. In addition, the strategy incorporated *Il13-gfp* transgene reporter mice to better localize the cell-type source of *Il13* gene expression. Together, these strategies defined *Il13* gene expression in ILC2s (at high levels per cell) and tissue macrophages (at relatively lower levels per cell as also found in eosinophils) using a combination of FACS with PCR-based assay and immunostaining for IL-13 expression and tissue immunostaining for GFP-reporter expression to enhance our previous analysis of lung macrophages (34-36). Together, the approach significantly extends evidence of IL-13 expression in mouse and human macrophages from our lab and other labs in the context of a type 2 immune response (34, 36, 64, 65). In particular, this full battery of assays provides a quantitative basis for the relative contributions of ILC2s versus tissue macrophages for the key IL-13 cytokine in the context of chronic disease. However, it is not yet possible to fully separate cytokine contributions of macrophages versus ILC2s because of another previously unrecognized control for ILC2 function.

This second feature of ILC2 function in chronic disease is the newly identified requirement for additional myeloid cell participation, separate from direct production of IL-13. Thus, we incorporated *wt/opT* to down-regulate the *Csf1*-dependent myeloid cells (particularly tissue macrophages) and thereby define the relative contributions to IL-13 production. As introduced above, this approach resulted in marked down-regulation of *Il13* gene expression and IL-13 protein production and in turn complete attenuation of chronic asthma-like lung disease after viral infection. Unexpectedly, we also found that *wt/opT* mice additionally manifested a marked down-regulation of ILC2 expansion and activation. The decreased activation included attenuation of ST2 expression via transcriptional and post-transcriptional regulation (the former based on decreased mRNA levels in *wt/opT* mice and the latter based on an increase in ST2 protein but not corresponding mRNA in ILC2s from *wild-type* mice and blockade of this increase in *wt/opT* mice). Comparable albeit lower level ST2 expression was also found in tissue macrophages after SeV infection, suggesting similar regulation of ST2 levels in this cell population. In that regard, the present results were also similar to the appearance of Trem-2 on tissue macrophages after SeV infection, again based on increases in protein with no change in corresponding mRNA levels (36). Together, the findings continue to highlight the role of post-transcriptional control of the type 2 immune response after viral infection but left unchecked how this or post-transcriptional control might occur.

This question was also resolved with unexpected findings. Thus, we generated a new *Il13-cherry* transgenic reporter mice given the role of IL-33-dependent signal transduction in

controlling IL-13 production (35). Based on study of this new mouse line, we learned that *Il33* gene expression was required for ILC2 accumulation and activation perhaps as expected, but also that *Il33* gene function was required for the transcriptional increase in *Il1rl1* mRNA and post-transcriptional up-regulation of ST2 on the surface of ILC2s during the development of chronic lung disease after viral infection. Moreover, this essential *Il33*-based signal was lost in *wt/opT* mice, thereby establishing an unrecognized role for *Csf1*-dependent myeloid cells in controlling ILC2 participation in the disease. Given that the major site for induction of *Il33* gene expression is localized to lung epithelial cells (particularly AT2 cells in this model and other models) (35, 52, 54, 55), the findings also implied that *Csf1*-dependent myeloid cell control of the epithelial cell-derived IL-33 was in turn responsible for ST2-dependent ILC2 activation. These findings are consistent with macrophage support of AT2 cell expansion found after helminth infection and other models of short-term tissue injury and repair (66-69). However, these previous models defined an effect of macrophages (often M2 macrophages) that is downstream of IL-13 production (67-69). Instead, in the present case, the *Csf1*-dependent myeloid cell effect is upstream of the epithelial cell to IL-33 production to ILC2 activation to IL-13 production axis that drives disease. We therefore propose that *Csf1*-dependent myeloid cells might represent an immune-cell niche for lung epithelial (likely AT2) cells. This aspect of regulating ILC2 function appears to have no clear precedent based on a review of previous work (70). Since this review was published, others have reported that *Csf1*-dependent macrophages are required for maintenance of Paneth cells and nearby stem cells in the intestinal epithelium (71) but full definition of the macrophage subset was not performed and no cytokine biology or disease model was studied. The present possibility for myeloid-lineage control of IL-33-expression in AT2 cells thereby significantly advances this concept.

Together, the present results provide a new framework as well as new questions for the development of progressive post-viral lung disease in particular and chronic inflammatory disease in general. Given the distinct nature of our findings, the myeloid cell effect on lung epithelial cells cannot yet be attributed to tissue macrophages versus another subset of the *Csf1*-dependent myeloid cell lineage. This issue still needs to be defined, most likely by identifying molecular factors that control *Csf1*-dependent myeloid cell activation and effector function in this setting and performing the corresponding loss-of-function and reconstitution experiments. Similarly, we still need to determine the precise epithelial cell target population and how it is regulated by myeloid-lineage cells during acute illness and chronic disease in the present model and in general. In that context, our study nonetheless provides a distinct cell and molecular axis from viruses to innate myeloid cells (a *Csf1*-dependent subset) to epithelial cells (likely an AT2 cell subset at least in mice) to innate lymphoid cells (an ILC2 subset) in the development of persistent inflammatory disease. In the present model, regulation of ST2 levels provides a key checkpoint for the development of long-term disease. It will therefore be of interest to revisit whether a similar molecular and/or cellular mechanism will also participate in the type 2 immune- response in related settings, e.g., allergy and parasitic infection. These comparisons will also define additional molecular interactions that drive this axis and thereby provide a therapeutic target for correcting the consequent inflammatory disease without interfering with host defense. Nonetheless, these findings already better explain the cellular context for ILC2 function and

the specialized need for myeloid cell cooperation for the development of a long-lasting type 2 immune response that allows progression from acute infectious illness to long-term lung disease. This type of post-viral disease resembles immunopathologic features found in asthma and COPD as well late events in the course of severe respiratory virus infections in general. Thus, post-viral lung disease can develop after severe infections due to respiratory syncytial virus, influenza virus, respiratory enterovirus, and coronavirus (CoV) in humans and animal models, including CoV outbreaks causing severe acute respiratory syndrome (SARS) and coronavirus disease of 2019 (COVID-19) (17, 37, 63, 72, 73). Therefore, defining pathogenesis and consequent therapeutic targets for progressive post-viral lung disease is critical to present and major public health concerns.

Acknowledgments

The authors thank Di Wu, Xiaohua Jin, and Rose Tidwell and the staff in the Siteman Flow Cytometry Core and Pulmonary Morphology Core for expert assistance.

This work was supported by grants from the National Institute of Allergy and Infectious Diseases (R01 AI130591), National Heart, Lung, and Blood Institute (R35 HL145242), and the Cystic Fibrosis Foundation.

Abbreviations used in this article:

AT2 cell	alveolar epithelial type 2 cell
ATCC	American Type Culture Collection
PFU	plaque-forming unit
ILC2	group 2 innate lymphoid cell
NP	nucleoprotein
PAS	periodic acid-Schiff
qPCR	quantitative PCR
MUC5AC	mucin 5AC
SeV	Sendai virus
ST2	suppressor of tumorigenicity 2

References

1. Vivier E, Artis D, Colonna M, Dieffenbach A, Di Santo JP, Eberl G, Koyasu S, Locksley RM, McKenzie ANJ, Mebius RE, Powrie F, and Spits H. 2018 Innate lymphoid cells: 10 years on. *Cell* 174: 1054–1066. [PubMed: 30142344]
2. Fort MM, Cheung J, Yen D, Li J, Zurawski SM, Lo S, Menon S, Clifford T, Hurst SD, Zurawski G, Leach MW, Gorman DM, and Rennick DM. 2001 IL-25 induces IL-4, IL-5, and IL-13 pathologies and Th2-associated pathologies in vivo. *Immunity* 15: 985–995. [PubMed: 11754819]
3. Hurst SD, Muchamuel T, Gorman DM, Gilbert JM, Clifford T, Kwan S, Menon S, Seymour B, Jackson C, Kung TT, Brieland JK, Zurawski SM, Chapman RW, Zurawski G, and Coffman RL. 2002 New IL-17 family members promote Th1 or Th2 responses in the lung: in vivo function of the novel cytokine IL-25. *J. Immunol* 169: 443–453. [PubMed: 12077275]

4. Fallon PG, Ballantyne SJ, Mangan NE, Barlow JL, Dasvarma A, Hewett DR, McIlgorm A, Jolin HE, and McKenzie ANJ. 2006 Identification of an interleukin (IL)-25-dependent cell population that provides IL-4, IL-5, and IL-13 at the onset of helminth expulsion. *J. Exp. Med* 203: 1105–1116. [PubMed: 16606668]
5. Moro K, Yamada T, Tanabe M, Takeuchi T, Ikawa T, Kawamoto H, Furusawa J, Ohtani M, Fujii H, and Koyasu S. 2010 Innate production of TH2 cytokines by adipose tissue-associated c-Kit+ Sca-1+ lymphoid cells. *Nature* 463: 540–544. [PubMed: 20023630]
6. Saenz SA, Siracusa MC, Perrigoue JG, Spencer SP, Urban JF Jr., Tocker JE, Budelsky AL, Kleinschek MA, Kastelein RA, Kambayashi T, Bhandoola A, and Artis D. 2010 IL-25 elicits a multi-potent progenitor cell population that promotes Th2 cytokine responses. *Nature* 464: 1362–1366. [PubMed: 20200520]
7. Neill DR, Wong SH, Bellosi A, Flynn RJ, Daly M, Langford TKA, Bucks C, Kane CM, Fallon PG, Pannell R, Jolin HE, and McKenzie ANJ. 2010 Nuocytes represent a new innate effector leukocyte that mediates type-2 immunity. *Nature* 464: 1367–1370. [PubMed: 20200518]
8. Price AE, Liang H-E, Sullivan BM, Reinhardt RL, Eisley CJ, Erle DJ, and Locksley RM. 2010 Systemically dispersed innate IL-13-expressing cells in type 2 immunity. *American Review of Respiratory Disease* 107: 11489–11494.
9. Mjosberg JM, Trifari S, Crellin NK, Peters CP, van Drunen CM, Piet B, Fokkens WJ, Cupedo T, and Spits H. 2011 Human IL-25- and IL-33-responsive type 2 innate lymphoid cells are defined by expression of CRTH2 and CD161. *Nat. Immunol* 12: 1055–1162. [PubMed: 21909091]
10. Barlow JL, Bellosi A, Hardman CS, Drynan LF, Wong SH, Cruickshank JP, and McKenzie ANJ. 2012 Innate IL-13-producing nuocytes arise during allergic lung inflammation and contribute to airways hyperreactivity. *J. Allergy Clin. Immunol* 129: 191–198. [PubMed: 22079492]
11. Christianson CA, Goplen NP, Zafar I, Irvin C, Good JTJ, Rollins DR, Gorentla B, Liu W, Gorska MM, Chu H, Martin RJ, and Alam R. 2015 Persistence of asthma requires multiple feedback circuits involving type 2 innate lymphoid cells and IL-33. *J. Allergy Clin. Immunol* 136: 59–68. [PubMed: 25617223]
12. Smith SG, Chen R, Kjarsgaard M, Huang C, Oliveria J-P, O’Byrne PM, Gauvreau GM, Boulet L-P, Lemiere C, Martin JG, Nair P, and Sehmi R. 2015 Increased numbers of activated group 2 innate lymphoid cells in the airways of patients with severe asthma and persistent airway eosinophilia. *J. Allergy Clin. Immunol* 137: 75–86. [PubMed: 26194544]
13. Halim TYF, Steer CA, Matha L, Gold MJ, Martinez-Gonzalez I, McNagny KM, McKenzie ANJ, and Takei F. 2014 Group 2 innate lymphoid cells are critical for the initiation of adaptive T helper 2 cell-mediated allergic lung inflammation. *Immunity* 40: 425–435. [PubMed: 24613091]
14. Guo L, Huang Y, Chen X, Hu-Li J, Urban JF Jr., and Paul WE. 2015 Innate immunological function of TH2 cells in vivo. *Nat. Immunol* 16: 1051–1059. [PubMed: 26322482]
15. Dhariwal J, Cameron A, Trujillo-Torralbo M-B, del Rosario A, Bakhsoliani E, Paulsen M, Jackson DJ, Edwards MR, Rana BMJ, Cousins DJ, Hansel TT, Johnston SL, and Walton RP. 2017 Mucosal type 2 innate lymphoid cells are a key component of the allergic response to aeroallergens. *Am. J. Respir. Crit. Care Med* 195: 1586–1596. [PubMed: 28085492]
16. Monticelli LA, Sonnenberg GF, Abt MC, Aleghat T, Ziegler CG, Doering TA, Angelosanto JM, Laidlaw BJ, Yang CY, Sathallyawal T, Kubota M, Turner D, Diamond JM, Goldrath AW, Farber DL, Collman RG, Wherry EJ, and Artis D. 2011 Innate lymphoid cells promote lung-tissue homeostasis after infection with influenza virus. *Nat. Immunol* 12: 1045–1054. [PubMed: 21946417]
17. Keeler SP, Agapov EV, Hinojosa ME, Letvin AN, Wu K, and Holtzman MJ. 2018 Influenza A virus infection causes chronic lung disease linked to sites of active viral RNA remnants. *J. Immunol* 201: 2354–2368. [PubMed: 30209189]
18. Salimi M, Barlow JL, Saunders SP, Xue L, Gutowska-Owsiak D, Wang X, Huang L-C, Johnson D, Scanlon ST, McKenzie ANJ, Fallon PG, and Ogg GS. 2013 A role for IL-25 and IL-33-driven type-2 innate lymphoid cells in atopic dermatitis. *J. Exp. Med* 210: 2939–2950. [PubMed: 24323357]
19. Walker JA, Oliphant CJ, Englezakis A, Yu Y, Clare S, Rodewald H-R, Belz G, Liu P, Fallon PG, and McKenzie ANJ. 2015 Bcl11b is essential for group 2 innate lymphoid cell development. *J. Exp. Med* 212: 875–882. [PubMed: 25964370]

20. Verhoef PA, Constantinides MG, McDonald BD, Urban JF Jr., Sperling AI, and Bendelac A. 2015 Intrinsic functional defects of type 2 innate lymphoid cells impair innate allergic inflammation in promyelocytic leukemia zinc finger (PLZF)-deficient mice. *J. Allergy Clin. Immunol* 2016: 591–600.
21. Huang Y, Guo L, Qiu J, Chen X, Hu-Li J, Siebenlist U, Williamson PR, Urban JF Jr., and Paul WE. 2015 IL-25-responsive, lineage-negative KLRG1hi cells are multipotential ‘inflammatory’ type 2 innate lymphoid cells. *Nat. Immunol* 16: 161–169. [PubMed: 25531830]
22. Lee M-W, Odegaard JI, Mukundan L, Qiu Y, Molofsky AB, Nussbaum JC, Yun K, Locksley RM, and Chawla A. 2015 Activated type 2 innate lymphoid cells regulate beige fat biogenesis. *Cell* 160: 1–14.
23. Klose CSN, Mahlakoiv T, Moeller JB, Rankin LC, Flamar A-L, Kabata H, Monticelli LA, Moriyama S, Garbes Putzel G, Rakhilin N, Shen X, Kostenis E, Konig GM, Senda T, Carpenter D, Farber DL, and Artis D. 2017 The neuropeptide neuromedin U stimulates innate lymphoid cells and type 2 inflammation. *Nature* 549: 282–286. [PubMed: 28869965]
24. Cardoso V, Chesne J, Ribeiro H, Garcia-Cassani B, Carvalho T, Bouchery T, Shah K, Barbosa-Morais NL, Harris N, and Veiga-Fernandes H. 2017 Neuronal regulation of type 2 innate lymphoid cells via neuromedin U. *Nature* 549: 277–281. [PubMed: 28869974]
25. Huang Y, Mao K, Chen X, Sun MA, Kawabe T, Li W, Usher N, Zhu J, Urban JF Jr., Paul WE, and Germain RN. 2018 S1P-dependent interorgan trafficking of group 2 innate lymphoid cells supports host defense. *Science* 359: 114–119. [PubMed: 29302015]
26. Monticelli LA, Buck MD, Flamar A-L, Saenz SA, Tait Wojno ED, Yudanin NA, Osborne LC, Hepworth MR, Tran SV, Rodewald H-R, Shah H, Cross JR, Diamond JM, Cantu E, Christie JD, Pearce EL, and Artis D. 2016 Arginase 1 is an innate lymphoid-cell-intrinsic metabolic checkpoint controlling type 2 inflammation. *Nat. Immunol* 17: 656–665. [PubMed: 27043409]
27. Moriyama S, Brestoff JR, Flamar A-L, Moeller JB, Klose CSN, Rankin LC, Yudanin NA, Monticelli LA, Putzel CG, Rodewald H-R, and Artis D. 2018 B2-adrenergic receptor-mediated negative regulation of group 2 innate lymphoid cell responses. *Science* 359: 1056–1061. [PubMed: 29496881]
28. Oliphant CJ, Hwang YY, Walker JA, Salimi M, Wong SH, Brewer JM, Englezakis A, Barlow JL, Hams E, Scanlon ST, Ogg GS, Fallon P, and McKenzie ANJ. 2014 MHCII-mediated dialog between group 2 innate lymphoid cells and CD(+) T cells potentiates type 2 immunity and promotes parasitic helminth expulsion. *Immunity* 41: 283–295. [PubMed: 25088770]
29. Halim TYF, Hwang YY, Scanlon ST, Zaghouani H, Garbi N, Fallon PG, and McKenzie ANJ. 2016 Group 2 innate lymphoid cells license dendritic cells to potentiate memory TH2 cell responses. *Nat. Immunol* 17.
30. Schlenner SM, Madan V, Busch K, Tietz A, Lauffle C, Costa C, Blum C, Jorg Fehling H, and Rodewald H-R. 2010 Fate mapping reveals separate origins of T cells and myeloid lineages in the thymus. *Immunity* 32: 426–436. [PubMed: 20303297]
31. Wong SH, Walker JA, Jolin HE, Drynan LF, Hams E, Camelo A, Barlow JL, Neill DR, Panova V, Koch U, Radtke F, Hardman CS, Hwang YY, Fallon PG, and McKenzie ANJ. 2012 Transcription factor RORa is critical for nuocyte development. *Nat. Immunol* 13: 229–236. [PubMed: 22267218]
32. Halim TYF, MacLaren A, Romanish MT, Gold MJ, McNagny KM, and Takei F. 2012 Retinoic-acid-receptor-related orphan nuclear receptor alpha is required for natural helper cell development and allergic inflammation. *Immunity* 37: 463–474. [PubMed: 22981535]
33. Dussault I, Fawcett D, Matthyssen A, Bader J-A, and Giguere V. 1998 Orphan nuclear receptor Rora-deficient mice display the cerebellar defects of staggerer. *Mechanisms of Dev* 70: 147–153.
34. Kim EY, Battaile JT, Patel AC, You Y, Agapov E, Grayson MH, Benoit LA, Byers DE, Alevy Y, Tucker J, Swanson S, Tidwell R, Tyner JW, Morton JD, Castro M, Polineni D, Patterson GA, Schwendener RA, Allard JD, Peltz G, and Holtzman MJ. 2008 Persistent activation of an innate immune response translates respiratory viral infection into chronic lung disease. *Nat. Med* 14: 633–640. [PubMed: 18488036]
35. Byers DE, Alexander-Brett J, Patel AC, Agapov E, Dang-Vu G, Jin X, Wu K, You Y, Alevy YG, Girard J-P, Stappenbeck TS, Patterson GA, Pierce RA, Brody SL, and Holtzman MJ. 2013 Long-term IL-33-producing epithelial progenitor cells in chronic obstructive lung disease. *J. Clin. Invest* 123: 3967–3982. [PubMed: 23945235]

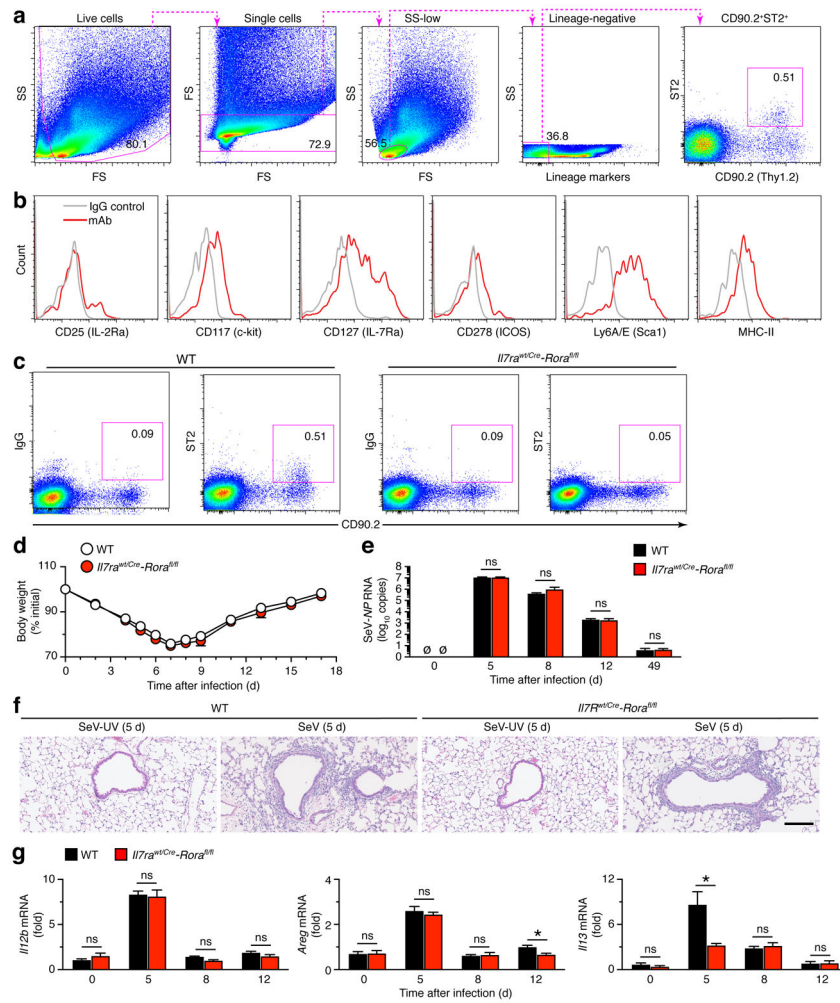
36. Wu K, Byers DE, Jin X, Agapov E, Alexander-Brett J, Patel AC, Cella M, Gilfilan S, Colonna M, Kober DL, Brett TJ, and Holtzman MJ. 2015 TREM-2 promotes macrophage survival and lung disease after respiratory viral infection. *J. Exp. Med* 212: 681–697. [PubMed: 25897174]
37. Zhang Y, Mao D, Keeler SP, Wang X, Wu K, Gerovac BJ, Shornick LP, Agapov E, and Holtzman MJ. 2019 Respiratory enterovirus (like parainfluenza virus) can cause chronic lung disease if protection by airway epithelial STAT1 is lost. *J. Immunol* 202: 2332–2347. [PubMed: 30804041]
38. Alevy Y, Patel AC, Romero AG, Patel DA, Tucker J, Roswit WT, Miller CA, Heier RF, Byers DE, Brett TJ, and Holtzman MJ. 2012 IL-13–induced airway mucus production is attenuated by MAPK13 inhibition. *J. Clin. Invest* 122: 4555–4568. [PubMed: 23187130]
39. Byers DE, Wu K, Dang-Vu G, Jin X, Agapov E, Zhang X, Battaile JT, Schechtman KB, Yusen R, Pierce RA, and Holtzman MJ. 2018 Triggering receptor expressed on myeloid cells-2 (TREM-2) expression tracks with M2-like macrophage activity and disease severity in COPD. *Chest* 153: 77–86. [PubMed: 29017955]
40. Chang Y, Kim HY, Albacker LA, Baumgarth N, McKenzie AN, Smith DE, Dekruyff RH, and Umetsu DT. 2011 Innate lymphoid cells mediate influenza-induced airway hyper-reactivity independently of adaptive immunity. *Nat. Immunol* 12: 631–638. [PubMed: 21623379]
41. Rajput C, Cui T, Han M, Lei J, Hinde JL, Wu Q, Kelley Bentley J, and Hershenson MB. 2017 Rora-dependent type 2 innate lymphoid cells are required and sufficient for mucous metaplasia in immature mice. *Am. J. Physiol. Lung Cell Mol. Physiol* 312: L983–L993. [PubMed: 28360114]
42. Stier MT, Bloodworth MH, Toki S, Newcomb DC, Goleniewska K, Boyd KL, QUITALIG M, Hotard AL, Moore ML, Hartert TV, Zhou B, McKenzie AN, and Peebles RSJ. 2016 Respiratory syncytial virus infection activates IL-13-producing group 2 innate lymphoid cells through thymic stromal lymphopoietin. *J. Allergy Clin. Immunol* 138: 814–824. [PubMed: 27156176]
43. Abboud SL, Woodruff K, Liu C, Shen V, and Ghosh-Choudhury N. 2002 Rescue of the osteopetrotic defect in op/op mice by osteoblast-specific targeting of soluble colony-stimulating factor-1. *Endocrinology* 143: 1942–1949. [PubMed: 11956177]
44. Zhang Y, Mao D, Roswit WT, Jin X, Patel AC, Patel DA, Agapov E, Wang Z, Tidwell RM, Atkinson JJ, Huang G, McCarthy R, Yu J, Yun NE, Paessler SL, Lawson TG, Omattage NS, Brett TJ, and Holtzman MJ. 2015 PARP9-DTX3L ubiquitin ligase targets host histone H2BJ and viral 3C protease to enhance interferon signaling and control viral infection. *Nat. Immunol* 16: 1215–1227. [PubMed: 26479788]
45. van Nunen MCJ, and van der Veen J. 1967 Experimental infection with Sendai virus in mice. *Arch Gesamte Virusforsch* 22: 388–397. [PubMed: 4300620]
46. Califano D, Cho JJ, Uddin MN, Lorentsen KJ, Yang Q, Bhandoola A, Li H, and Avram D. 2015 Transcription factor Bcl11b controls identity and function of mature type 2 innate lymphoid cells. *Immunity* 43: 354–368. [PubMed: 26231117]
47. Ricardo-Gonzalez RR, Van Dyken SJ, Schneider C, Lee J, Nussbaum JC, Liang HE, Vaka D, Eckalbar WL, Molofsky AB, Erle DJ, and Locksley RM. 2018 Tissue signals imprint ILC2 identity with anticipatory function. *Nat. Immunol* 19: 1093–1099. [PubMed: 30201992]
48. Walter MJ, Kajiwarra N, Karanja P, Castro M, and Holtzman MJ. 2001 IL-12 p40 production by barrier epithelial cells during airway inflammation. *J. Exp. Med* 193: 339–352. [PubMed: 11157054]
49. Look DC, Walter MJ, Williamson MR, Pang L, You Y, Sreshta JN, Johnson JE, Zander DS, and Brody SL. 2001 Effects of paramyxoviral infection on airway epithelial cell Foxj1 expression, ciliogenesis, and mucociliary function. *Am. J. Pathol* 159: 2055–2069. [PubMed: 11733356]
50. Walter MJ, Morton JD, Kajiwarra N, Agapov E, and Holtzman MJ. 2002 Viral induction of a chronic asthma phenotype and genetic segregation from the acute response. *J. Clin. Invest* 110: 165–175. [PubMed: 12122108]
51. Jacobsen EA, Helters RA, Lee JJ, and Lee NA. 2012 The expanding role(s) of eosinophils in health and disease. *Blood* 120: 3882–3890. [PubMed: 22936660]
52. Hardman CS, Panova V, and McKenzie ANJ. 2012 IL-33 citrine reporter mice reveal the temporal and spatial expression of IL-33 during allergic lung inflammation. *Eur. J. Immunol* 43: 1–11.

53. Stier MT, Zhang J, Goleniewska K, Cephus JY, Rusznak M, Wu L, Van Kaer L, Zhou B, Newcomb DC, and Peebles RS Jr. 2019 IL-33 promotes the egress of group 2 innate lymphoid cells from bone marrow. *J. Exp. Med* 215: 263–281.
54. Pichery M, Mirey E, Mercier P, Lefrancais E, Dujardin A, Ortega N, and Girard J-P. 2012 Endogenous IL-33 is highly expressed in mouse epithelial barrier tissues, lymphoid organs, brain, embryos, and inflamed tissues: in situ analysis using a novel Il-33-LacZ gene trap reporter strain. *J. Immunol* 188: 3488–3495. [PubMed: 22371395]
55. Mohapatra A, Van Dyken SJ, Schneider C, Nussbaum JC, Liang H-E, and Locksley RM. 2016 Group 2 innate lymphoid cells utilize the IRF4-IL-9 module to coordinate epithelial cell maintenance of lung homeostasis. *Mucosal immunology* 9: 275–286. [PubMed: 26129648]
56. Califano D, Furuya Y, Roberts S, Avram D, McKenzie ANJ, and Metzger DW. 2018 IFN-g increases susceptibility to influenza A infection through suppression of group II innate lymphoid cells. *Mucosal immunology* 11: 209–219. [PubMed: 28513592]
57. Bagnasco D, Caminati M, Ferrando M, Aloe T, Testino E, Canonica GW, and Passalacqua G. 2018 Anti-IL-5 and IL-5Ra: efficacy and safety of new therapeutic strategies in severe uncontrolled asthma. *BioMed Research International* 2018:5698212: 1–8.
58. Chen Y-L, Gutowska-Owsiak D, Hardman CS, Westmoreland M, MacKenzie T, Cifuentes L, Waithe D, Lloyd-Lavery A, Marquette A, Londei M, and Ogg G. 2019 Proof-of-concept clinical trial of etokimab shows a key role for IL-33 in atopic dermatitis pathogenesis. *Sci. Transl. Med* 11.
59. Chinthrajah S, Cao S, Liu C, Lyu S-C, Sindher SB, Long A, Sampath V, Petroni D, Londei M, and Nadeau KC. 2019 Phase 2a randomized, placebo-controlled study of anti-IL-33 in peanut allergy. *JCI Insight* 4: e131347.
60. Jouanguy E, Lamhamedi-Cherradi S, Lammas D, Dorman SE, Fondaneche M-C, Dupuis S, Doffinger R, Altare F, Girdlestone J, Emile J-F, Ducoulombier H, Edgar D, Clarke J, Oxelius V-A, Brai M, Novelli V, Heyne K, Fischer A, Holland SM, Kumararatne S, Schreiber RD, and Casanova J-L. 1999 A human IFNGR1 small deletion hotspot associated with dominant susceptibility to mycobacterial infection. *Nat. Genet* 21: 370–378. [PubMed: 10192386]
61. Vely F, Barlogis V, Vallentin B, Neven B, Piperoglou C, Ebbo M, Perchet T, Petit M, Yessaad N, Touzot F, Bruneau J, Mahlaoui N, Zucchini N, Farnarier C, Michel G, Moshous D, Blanche S, Dujardin A, Spits H, Distler JHW, Ramming A, Picard C, Golub R, Fischer A, and Vivier E. 2016 Evidence of innate lymphoid cell redundancy in humans. *Nat. Immunol* 17: 1291–1299. [PubMed: 27618553]
62. Martinez FJ, Han MK, Allinson JP, Barr RG, Boucher RC, Claverley PMA, Celli BR, Christenson SA, Crystal RG, Fageras M, Freeman CM, Groenke L, Hoffman EA, Kesimer M, Kostikas K, Paine R, Raffi S, Rennard SI, Segal LN, Shaykhiev R, Stevenson C, Tal-Singer R, Vestbo J, Woodruff PG, Curtis JL, and Wedzicha JA. 2018 At the root: defining and halting progression of early chronic obstructive pulmonary disease. *Am. J. Respir. Crit. Care Med* 197: 1540–1551. [PubMed: 29406779]
63. Vu LD, Siefker D, Jones TL, You D, Taylor R, DeVincenzo JP, and Cormier SA. 2019 Elevated levels of type 2 respiratory innate lymphoid cells in human infants with severe RSV bronchiolitis. *Am. J. Respir. Crit. Care Med* 200: 1414–1423. [PubMed: 31237777]
64. Chung Y, Hong JY, Lei J, Chen Q, Bentley JK, and Hershenson MB. 2015 Rhinovirus infection induces interleukin-13 production from CD11b-positive, M2-polarized exudative macrophages. *Am. J. Respir. Cell Mol. Biol* 52: 205–216. [PubMed: 25029349]
65. Yang Z, Grinchuk V, Urban JF Jr., Bohl J, Sun R, Notari L, Yan S, Ramalingam T, Keegan AD, Wynn TA, Shea-Donohue T, and Zhao A. 2013 Macrophages as IL-24/IL-33-responsive cells play an important role in the induction of type 2 immunity. *PloS ONE* 8: e59441. [PubMed: 23536877]
66. Hung L-Y, Sen D, Oniskey TK, Katzen J, Cohen NA, Vaughan AE, Nieves W, Urisman A, Beers MF, Krummel MF, and Herbert DR. 2018 Macrophages promote epithelial proliferation following infectious and non-infectious lung injury through a Trefoil factor 2-dependent mechanism. *Mucosal immunology* 12: 64–76. [PubMed: 30337651]
67. Lechner AJ, Driver IH, Lee J, Conroy CM, Nagle A, Locksley RM, and Rock JR. 2017 Recruited monocytes and type 2 immunity promote lung regeneration following pneumonectomy. *Cell Stem Cell* 21: 120–134. [PubMed: 28506464]

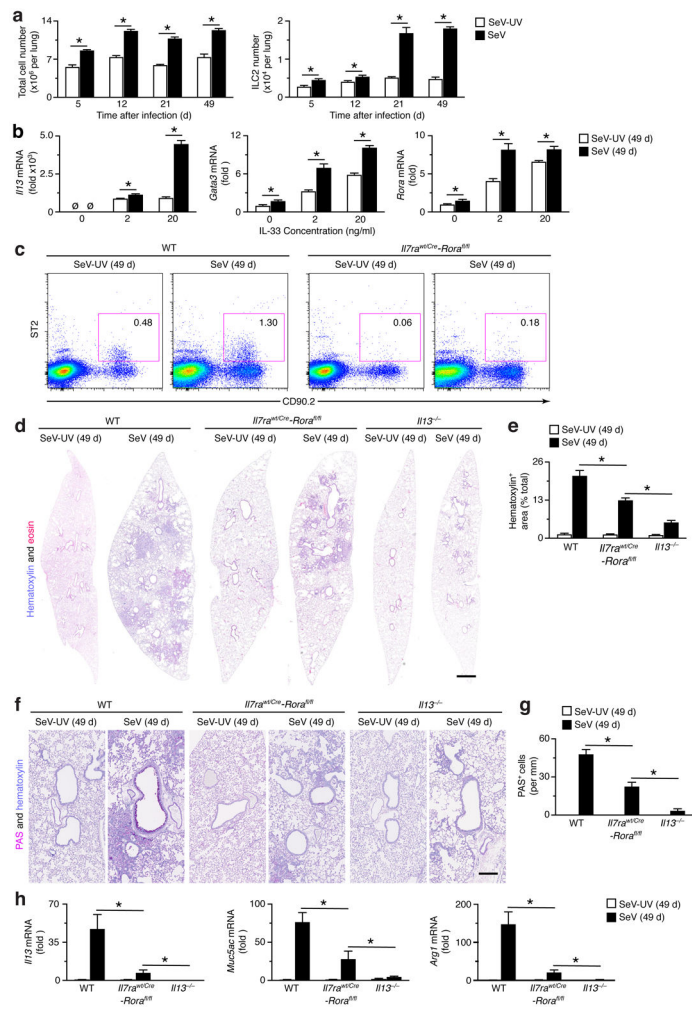
68. Shiraishi M, Shintani Y, Shintani Y, Ishida H, Saba R, Yamaguchi A, Adachi H, Yashiro K, and Suzuki K. 2016 Alternatively activated macrophages determine repair of the infarcted adult murine heart. *J. Clin. Invest* 126: 2151–2166. [PubMed: 27140396]
69. Bosurgi L, Cao YG, Cabeza-Cabrerizo M, Tucci A, Hughes LD, Y. K, Weinstein JS, Licona-Limon P, Schmid ET, Pelorosso F, Gagliani N, Craft JE, Flavell RA, Ghosh S, and Rothlin CV. 2017 Macrophage function in tissue repair and remodeling requires IL-4 or IL-13 with apoptotic cells. *Science* 356.
70. Gieseck RL, Wilson MS, and Wynn TA. 2017 Type 2 immunity in tissue repair and fibrosis. *Nat. Rev. Immunol* in press.
71. Sehgal A, Donaldson DS, Pridans C, Sauter KA, Hume DA, and Mabbott NA. 2018 The role of CSF1R-dependent macrophages in control of the intestinal stem-cell niche. *Nat. Comm* 9: 1272.
72. Page C, Goicochea L, Matthews K, Zhang Y, Klover P, Holtzman MJ, Hennighausen L, and Frieman M. 2012 Induction of alternatively activated macrophages enhances pathogenesis during severe acute respiratory syndrome coronavirus infection. *J. Virol* 86: 13334–13349. [PubMed: 23015710]
73. Barton LM, Duval EJ, Stroberg E, Ghosh S, and Mukhopadhyay S. 2020 COVID-19 autopsies, Oklahoma, USA. *Am J Clin Pathol* 153: 725–733. [PubMed: 32275742]

Key points:

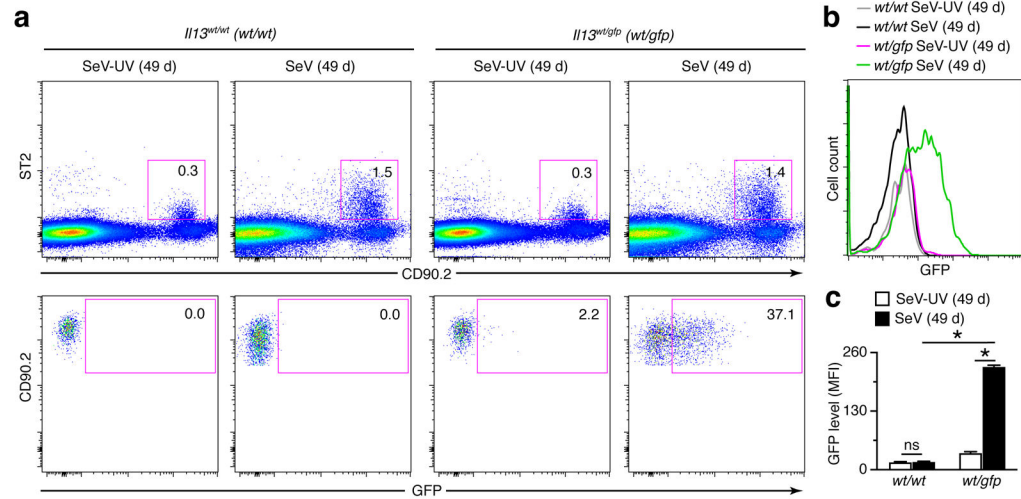
1. ILC2s are activated even after injury from respiratory viral infection is resolved.
2. ILC2s contribute to a chronic type 2 immune-response after viral infection.
3. ILC2s depend on myeloid-macrophage lineage cells to drive post-viral disease.

**FIGURE 1.**

ILC2s do not influence acute illness after viral infection. **(a)** Flow cytometry scheme for analysis of ILC2s in lungs from wild-type C57BL/6J (WT) mice assessed at baseline without infection. Lineage markers are CD11c, NK1.1, CD3e, CD45R/B220, CD11b, TER-119, and Ly6G/6C. **(b)** Expression of biomarkers in lung ILC2 (CD90.2⁺ST2⁺) population from WT mice at baseline. **(c)** Flow cytograms for levels of ILC2s from lungs of WT and *Il7ra^{wt/Cre}-Rora^{fl/fl}* mice at baseline. Values indicate percentage of cells in the corresponding gate. **(d)** Body weights at indicated times after infection with SeV in WT and *Il7ra^{wt/Cre}-Rora^{fl/fl}* mice. **(e)** Corresponding viral loads in lungs for conditions in (d). **(f)** Hematoxylin and eosin staining of lung sections for indicated conditions. Scale bar, 500 μ m. **(g)** Levels of mRNA expression in lungs from WT and *Il7ra^{wt/Cre}-Rora^{fl/fl}* mice at indicated times after SeV infection. All data are representative of three separate experiments (mean and s.e.m.) with at least 5 mice per condition in each experiment. * P <0.01.

**FIGURE 2.**

ILC2s do not fully account for chronic lung disease after viral infection. **(a)** Levels of total cells and ILC2s in the lungs of WT mice at indicated times after infection with SeV or SeV-UV as determined by flow cytometry. **(b)** Levels of ILC2 markers (*I13*, *Gata3*, and *Rora*) mRNA in ILC2s that were FACS-isolated from lung and treated with IL-33 (0–20 ng/ml). **(c)** Cytograms for ILC2s (Lin[−]CD90.2⁺ST2⁺) in WT and *Il7r^{wu/Cre}-Rora^{fl/fl}* mice at 49 d after SeV or SeV-UV. **(d)** Hematoxylin and eosin staining of full-lung sections from indicated mouse strains at 49 d after SeV or SeV-UV. **(e)** Quantitation of tissue staining in (d) using image-analysis software. **(f)** PAS and hematoxylin staining of lung sections for conditions in (d). **(g)** Quantitation of tissue staining in (f). **(h)** Levels of indicated mRNAs in lung tissue for conditions in (d). All data are representative of three separate experiments (mean and s.e.m.) with at least 5 mice per condition in each experiment. **P*<0.01.

**FIGURE 3.**

ILC2s contribute to chronic IL-13 production after viral infection based on *Il13* reporter gene expression. **(a)** Flow cytograms for ILC2s ($\text{Lin}^- \text{CD90.2}^+ \text{ST2}^+ \text{GFP}^+$) and GFP-expressing ILC2s ($\text{Lin}^- \text{CD90.2}^+ \text{ST2}^+ \text{GFP}^+$) in lungs of *Il13^{wt/wt} (wt/wt)* and *Il13^{wt/gfp} (wt/gfp)* mice at 49 d after SeV or SeV-UV. **(b)** Histograms for ILC2s ($\text{Lin}^- \text{CD90.2}^+ \text{ST2}^+$) in lungs of *Il13^{wt/wt}* and *Il13^{wt/gfp}* mice at 49 d after infection with SeV or SeV-UV based on GFP signal detection. **(c)** Levels of IL-13-GFP based on MFI for conditions in (b). All data are representative of three separate experiments (mean and s.e.m.) with at least 5 mice per condition in each experiment. * $P < 0.01$.

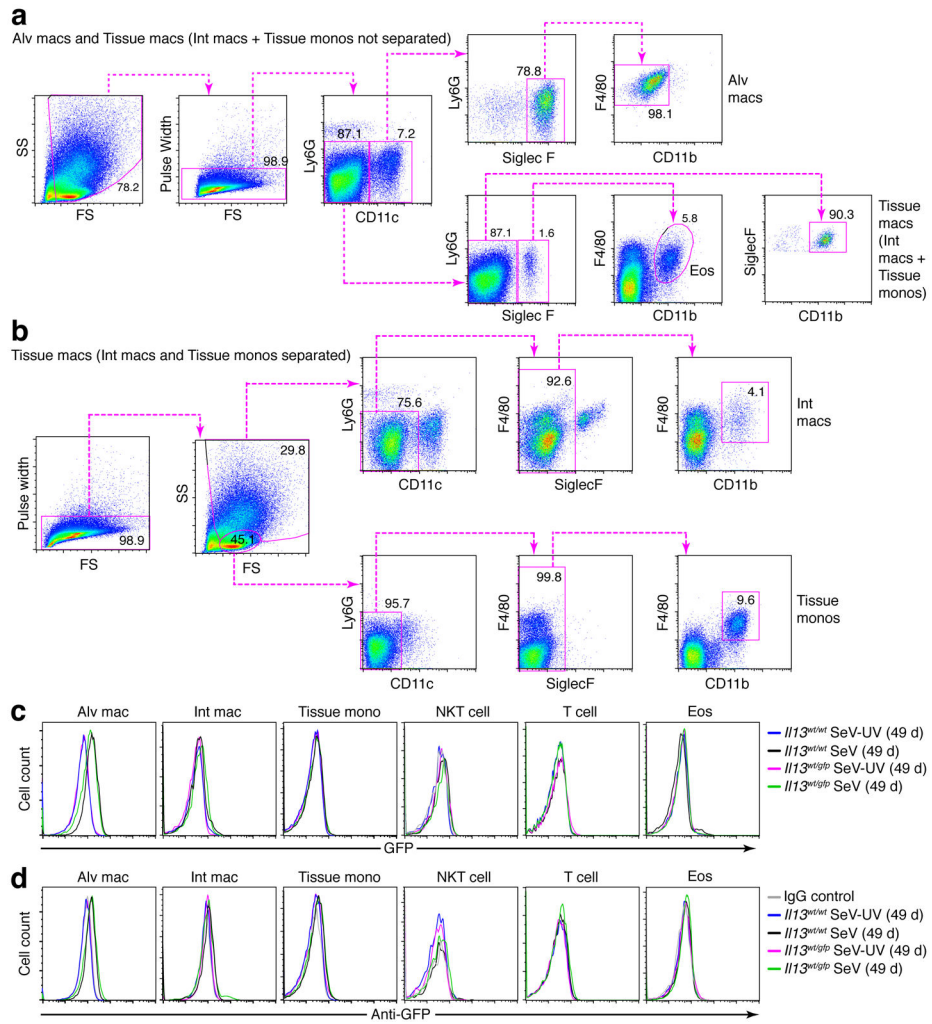
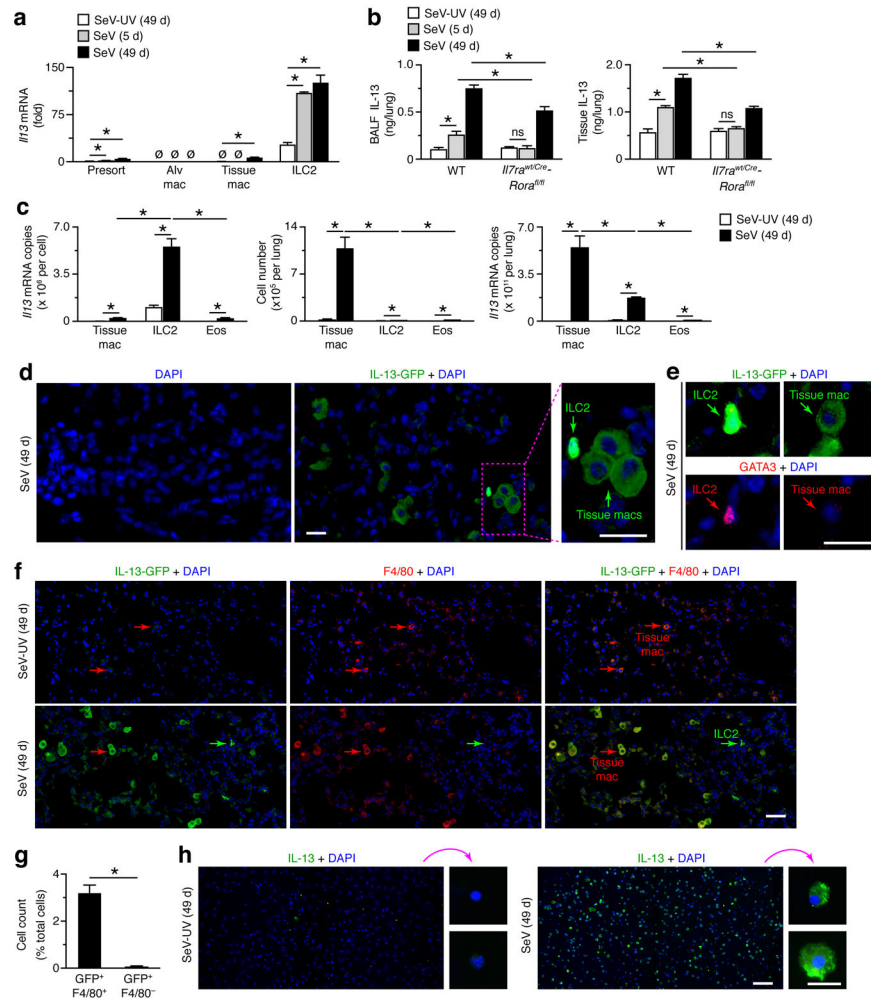


FIGURE 4. IL-13-GFP reporter expression is not detectable on lung macrophage or non-ILC2 lymphoid populations after viral infection. **(a)** Cytograms for analysis of alveolar macrophages (Ly6G⁻CD11c⁺Siglec-F⁺F4/80⁺CD11b⁻), eosinophils (eos; Ly6G⁻CD11c⁻Siglec-F⁺F4/80⁺CD11b⁺), and tissue macrophages (Ly6G⁻CD11c⁻Siglec-F⁻F4/80⁺CD11b⁺) in lung tissue from WT mice at 49 d after SeV infection. **(b)** Cytograms for analysis of tissue macrophages separately as interstitial macrophages (SS^{high}Ly6G⁻CD11c⁻F4/80⁺CD11b⁺) or tissue monocytes (SS^{low}Ly6G⁻CD11c⁻F4/80⁺CD11b⁺) for conditions in (a). **(c)** Histograms for analysis of IL-13-GFP expression in indicated macrophage and lymphocyte populations (NKT cells as SS^{low}CD3e⁺NK1.1⁺ and T cells as SS^{low}CD3e⁺) and eosinophils from lungs of *Il13^{wl/wl}* and *Il13^{wl/gfp}* mice at 49 d after SeV or SeV-UV. Detection was based on GFP fluorescence signal. **(d)** Corresponding histograms for conditions in (c), except that detection was based on anti-GFP mAb. All data are representative of three separate experiments with 5 mice per condition in each experiment. **P*<0.01.

**FIGURE 5.**

ILC2s need tissue macrophages to account for chronic IL-13 production after viral infection. (a) Levels of *I13* mRNA in FACS-isolated alveolar macrophage (Alv mac), tissue macrophage, ILC2, and lung epithelial cell (CD45⁻CD31⁻EpCAM⁺) populations from WT mice at 5 and 49 d after infection with SeV or SeV-UV. (b) Levels of IL-13 in bronchoalveolar lavage fluid (BALF) and lung tissue in WT and *Il7ra^{wtCre}-Rora^{fl/fl}* mice for conditions in (a). (c) Levels of *I13* mRNA in tissue macrophage, ILC2, and eosinophil populations that were FACS-isolated from lungs of WT mice at 49 d after SeV or SeV-UV with results expressed as *I13* mRNA copies per cell and as *I13* mRNA copies per lung (copies per cell x number of cells per lung). (d) Immunostaining for IL-13-GFP alone and with DAPI counterstaining in lung sections from *I13^{wt/gfp}* mice at 49 d after SeV. Arrows indicate representative ILC2 and tissue macrophage morphology and staining intensity. Scale bar, 100 μ m. (e) Immunostaining for IL-13-GFP and GATA-3 for conditions in (d). Scale bar, 50 μ m. (f) Immunostaining for IL-13-GFP (using anti-GFP Ab) and F4/80 with DAPI counterstaining in lung sections from *I13^{wt/gfp}* mice at 49 d after SeV or SeV-UV. Arrows indicate examples of GFP⁻F4/80⁺ and GFP⁺F4/80⁺ tissue macrophages and GFP⁺F4/80⁻ ILC2. Scale bar, 100 μ m. (g) Quantitation of immunostaining in (f). (h)

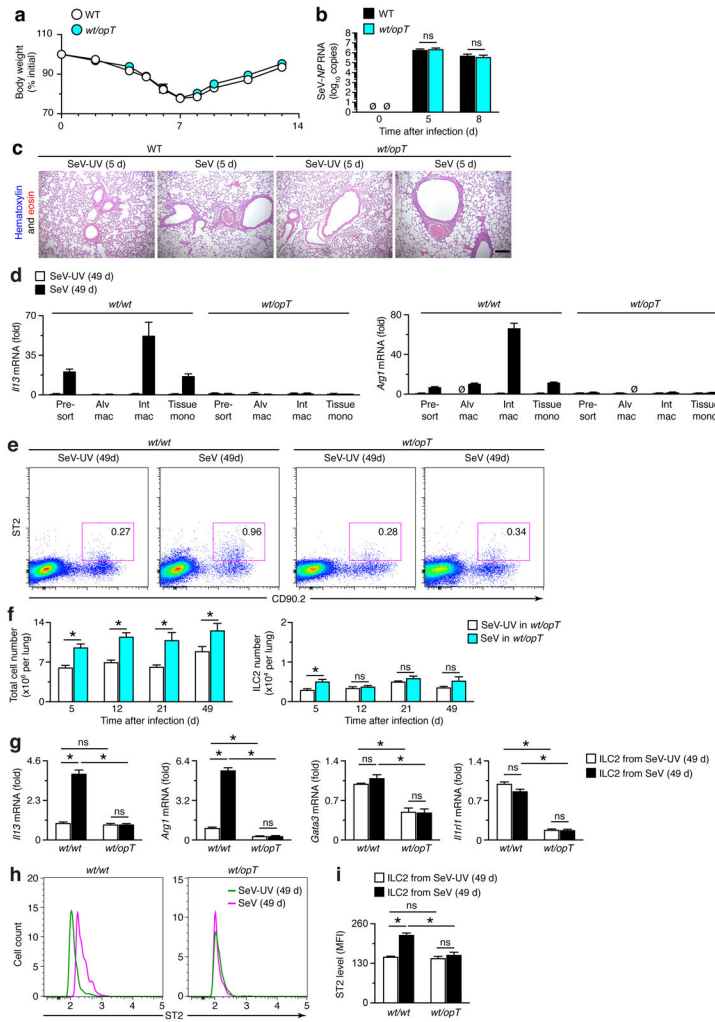
Immunostaining for IL-13 (using anti-IL-13 Ab) in tissue macrophages that were FACS-isolated from WT mice at 49 d after SeV or SeV-UV. All data are representative of three separate experiments (mean and s.e.m.) with at least 5 mice per condition in each experiment. * $P < 0.01$.

Author Manuscript

Author Manuscript

Author Manuscript

Author Manuscript

**FIGURE 6.**

Tissue macrophages regulate ILC2 accumulation and activation in chronic lung disease after viral infection. **(a)** Body weights at indicated times after infection with SeV in WT and *wt/opT* mice. **(b)** Corresponding viral loads in lungs for conditions in (a). **(c)** Hematoxylin and eosin staining of lung sections for indicated conditions. Scale bar, 500 μm . **(d)** Levels of *Il13* and *Arg1* mRNA in FACS-isolated macrophage populations from lungs of *wt/wt* and *wt/opT* mice at 49 d after SeV or SeV-UV. **(e)** Flow cytograms for ILC2s from *wt/wt* and *wt/opT* mice at 49 d after SeV or SeV-UV. **(f)** Quantitation of total cell and ILC2 levels from lungs of *wt/opT* mice at 5-49 d after SeV or SeV-UV using flow cytometry conditions in (e). **(g)** Levels of *Il13*, *Gata3*, *Arg1*, and *Il1rl1* mRNA in FACS-isolated ILC2s from *wt/wt* and *wt/opT* mice at 49 d after SeV or SeV-UV. **(h)** Flow histograms for ST2 expression in ILC2s from lungs of *wt/wt* and *wt/opT* mice at 49 d after SeV infection or SeV-UV. **(i)** Levels of ST2 based on MFI for conditions in (h). All data are representative of three separate experiments (mean and s.e.m.) with at least 5 mice per condition in each experiment. * $P < 0.01$.

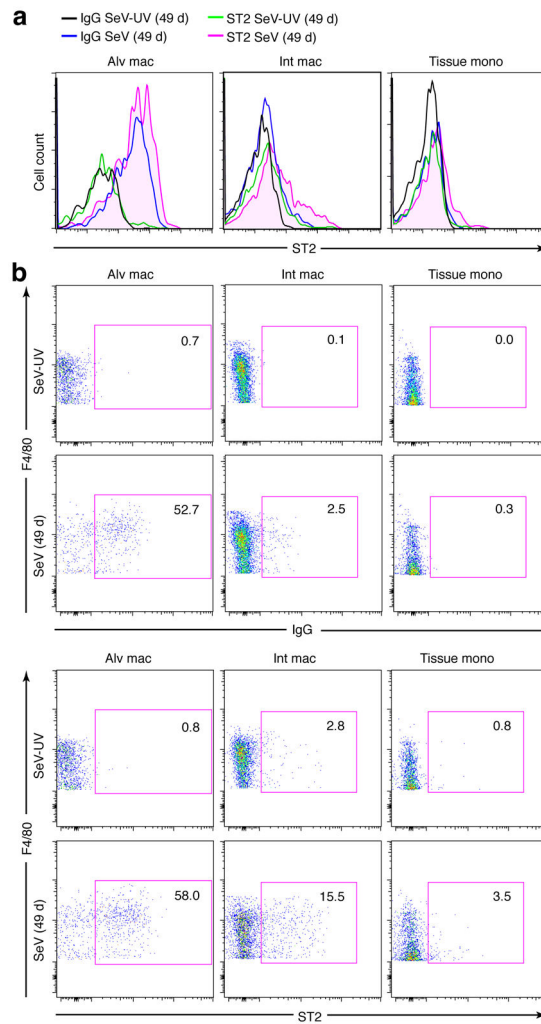
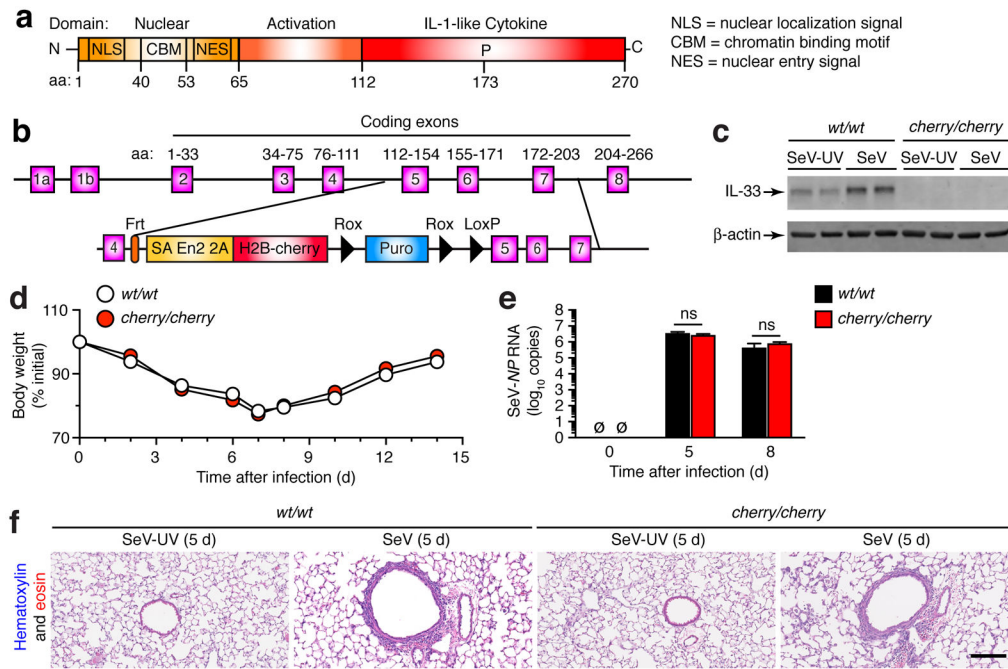
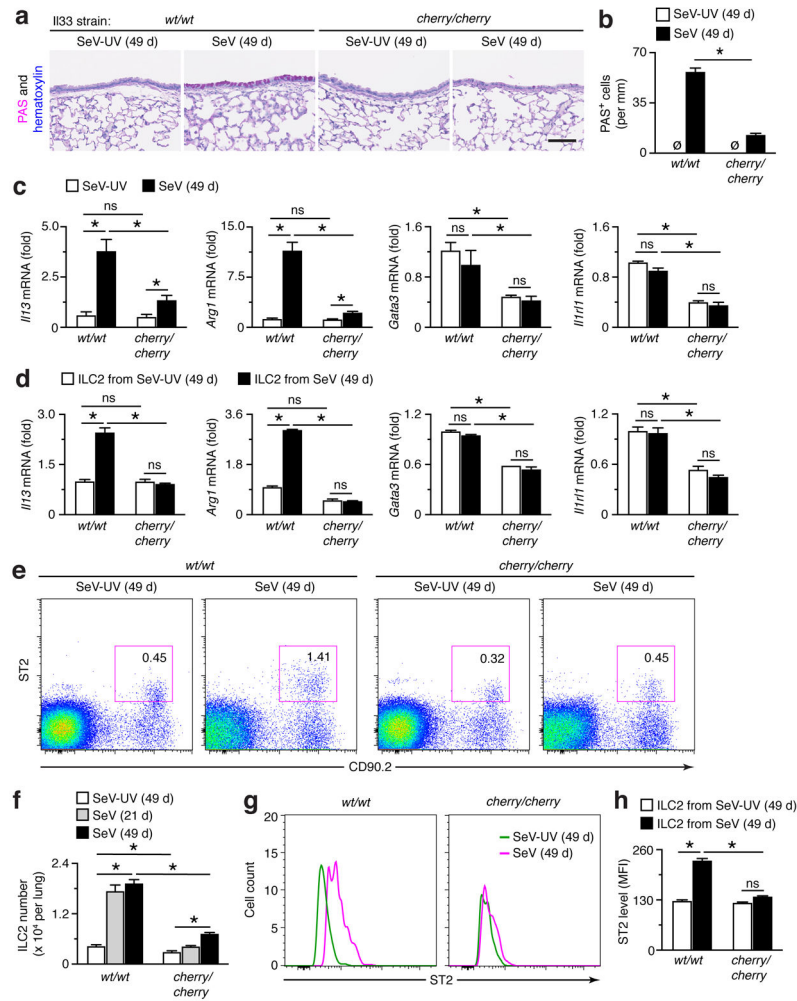


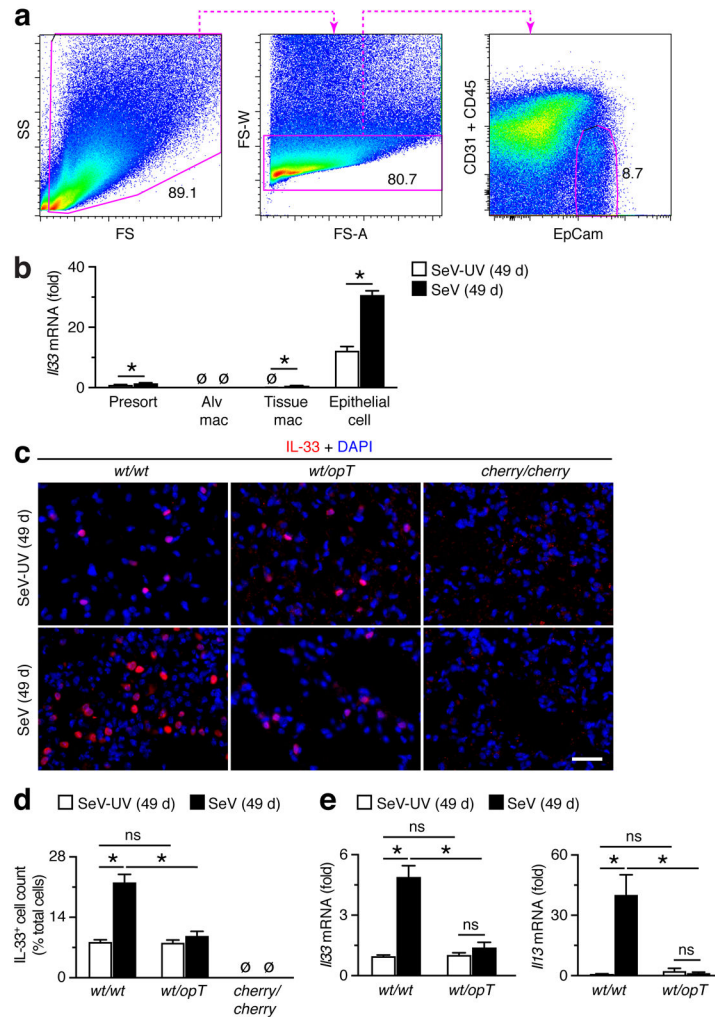
FIGURE 7. ST2 expression is detectable on a subset of tissue macrophages after viral infection. **(a)** Histograms for analysis of ST2 expression in indicated macrophage populations from lungs of WT mice at 49 d after SeV infection or SeV-UV. Detection was based on anti-ST2 mAb or IgG control. **(b)** Corresponding cytochrome plots for conditions in **(a)**. Data are representative of three separate experiments with 5 mice per condition in each experiment.

**FIGURE 8.**

Generation and phenotype of *Il33*-cherry transgenic reporter mice reveals no effect of *Il33* gene expression on acute illness after viral infection. (a) Scheme for domain structure of mouse IL-33 protein. (b) Scheme for targeting construct for generating IL-33-cherry reporter mice (*Il33*^{cherry/cherry}). (c) Western blot for IL-33 levels in lung tissue from *Il33*^{wt/wt} (*wt/wt*) and *Il33*^{cherry/cherry} (*cherry/cherry*) mice at 49 d after infection with SeV or SeV-UV. (d) Body weights at indicated times after infection with SeV in *Il33*^{wt/wt} and *Il33*^{cherry/cherry} mice. (e) Corresponding viral loads in lungs for conditions in (d). (f) Hematoxylin and eosin staining of lung sections for indicated conditions. Scale bar, 500 μm. All data are representative of three separate experiments (mean and s.e.m.) with at least 5 mice per condition in each experiment.

**FIGURE 9.**

Phenotype of *I133-cherry* transgenic reporter mice demonstrates *I133* gene function for ILC2 activation and accumulation during chronic post-viral lung disease. **(a)** PAS and hematoxylin staining of lung sections from *wt/wt* and *cherry/cherry* mice at 49 d after SeV or SeV-UV. Scale bar, 200 μ m. **(b)** Quantitation of PAS⁺ cells for conditions in (a). **(c)** Levels of indicated mRNAs in lungs from *wt/wt* and *cherry/cherry* mice at 49 d after SeV or SeV-UV. **(d)** Levels of indicated mRNAs in ILC2s isolated from lungs of *wt/wt* and *cherry/cherry* mice at 49 d after SeV or SeV-UV. **(e)** Flow cytograms for ILC2s in *wt/wt* and *cherry/cherry* mice at 49 d after SeV or SeV-UV. **(f)** Quantitation of ILC2 levels in *wt/wt* and *cherry/cherry* mice at 21 and 49 d after SeV and at 49 d after SeV-UV using flow cytometry conditions in (e). **(g)** Flow histograms for ST2 expression in ILC2s from lungs of *wt/wt* and *cherry/cherry* mice at 49 d after SeV or SeV-UV. **(h)** Levels of ST2 based on MFI for conditions in (g). All data are representative of three separate experiments (mean and s.e.m.) with at least 5 mice per condition in each experiment. * $P < 0.01$.

**FIGURE 10.**

Lung *Csf1*-dependent myeloid cells are required for induction of *Il33* gene expression in lung epithelial cells after viral infection. **(a)** Cytograms for analysis of lung epithelial cells ($CD45^{-}CD31^{-}EpCAM^{+}$) in lung tissue from WT mice at 49 d after SeV infection. **(b)** Levels of *Il33* mRNA in FACS-isolated populations of macrophages and epithelial cells from lungs of *wt/wt* mice at 49 d after SeV or SeV-UV. **(c)** Immunostaining for IL-33 in lung sections from *wt/wt*, *wt/opT*, and control *Il33*-deficient *cherry/cherry* mice at 49 d after SeV or SeV-UV. Scale bar, 200 μ m. **(d)** Quantitation of IL-33⁺ cells for conditions in (c). **(e)** Levels of *Il33* and *Il13* mRNA in lungs of *wt/wt* and *wt/opT* mice at 49 d after SeV or SeV-UV. Data are representative of three separate experiments with at least 5 mice per condition in each experiment. * $P < 0.01$.

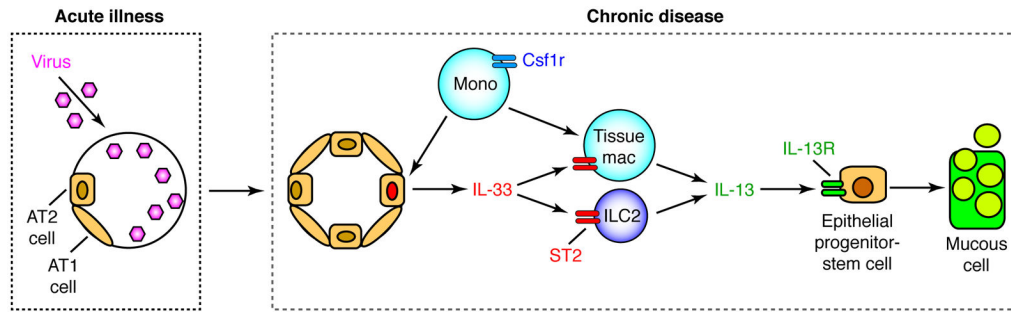


FIGURE 11.

Scheme for *Csf1*-dependent myeloid cell inputs to ILC2 function in chronic disease after respiratory viral infection. Sequential steps in the scheme include: (1) acute illness with damage to host cells, including progenitor AT2 cells and daughter alveolar epithelial type 1 (AT1) cells; (2) subsequent replacement of these populations including AT2 cells that provide increased IL-33 to activate ILC2 production of IL-13 and in turn IL-13R-dependent differentiation of epithelial stem cells into mucous cells. The *Csf1*-dependent myeloid cells act upstream for induction of *Il33* gene expression and downstream to provide tissue macrophages for additional *Il13* gene expression that is required for full development of chronic lung disease after viral infection.